

Variable stars in Local Group Galaxies - II. Sculptor dSph

C. E. Martínez-Vázquez^{1,2,*}, P. B. Stetson³, M. Monelli^{1,2}, E. J. Bernard⁴, G. Fiorentino⁵,
C. Gallart^{1,2}, G. Bono^{6,7}, S. Cassisi⁸, M. Dall’Ora⁹, I. Ferraro⁷, G. Iannicola⁷, and
A. R. Walker¹⁰

¹ *Instituto de Astrofísica de Canarias (IAC), E-38205 La Laguna, Tenerife, Spain*

² *Universidad de La Laguna (ULL), Dpto. Astrofísica, E-38206 La Laguna, Tenerife, Spain*

³ *Herzberg Astronomy and Astrophysics, National Research Council Canada, 5071 West Saanich Road, Victoria, BC V9E 2E7, Canada*

⁴ *Laboratoire Lagrange, Observatoire de la Côte d’Azur, 06304 Nice Cedex 4, France*

⁵ *INAF-Osservatorio Astronomico di Bologna, via Ranzani 1, 40127, Bologna, Italy*

⁶ *Dipartimento di Fisica, Università di Roma Tor Vergata, Via della Ricerca Scientifica 1, 00133 Roma, Italy*

⁷ *INAF-Osservatorio Astronomico di Roma, Via Frascati 33, 00040 Monteporzio Catone, Italy*

⁸ *INAF-Osservatorio Astronomico di Teramo, Via M. Maggini, 64100 Teramo, Italy*

⁹ *INAF-Osservatorio Astronomico di Capodimonte, Via Moiariello 16, 80131 Napoli, Italy*

¹⁰ *Cerro Tololo Inter-American Observatory, National Optical Astronomy Observatory, Casilla 603, La Serena, Chile*

Accepted 2016 July 28. Received 2016 July 28; in original form 2016 March 31

ABSTRACT

We present the identification of 634 variable stars in the Milky Way dSph satellite Sculptor based on archival ground-based optical observations spanning ~ 24 years and covering ~ 2.5 deg². We employed the same methodologies as the “Homogeneous Photometry” series published by Stetson. In particular, we have identified and characterized one of the largest (536) RR Lyrae samples so far in a Milky Way dSph satellite. We have also detected four Anomalous Cepheids, 23 SX Phoenicis stars, five eclipsing binaries, three field variable stars, three *peculiar* variable stars located above the horizontal branch – near to the locus of BL Herculis – that we are unable to classify properly. Additionally we identify 37 Long Period Variables plus 23 probable variable stars, for which the current data do not allow us to determine the period. We report positions and finding charts for all the variable stars, and basic properties (period, amplitude, mean magnitude) and light curves for 574 of them. We discuss the properties of the RR Lyrae stars in the Bailey diagram, which supports the coexistence of subpopulations with different chemical compositions. We estimate the mean mass of Anomalous Cepheids ($\sim 1.5M_{\odot}$) and SX Phoenicis stars ($\sim 1M_{\odot}$). We discuss in detail the nature of the former. The connections between the properties of the different families of variable stars are discussed in the context of the star formation history of the Sculptor dSph galaxy.

Key words: stars: variables: general – galaxies: evolution – galaxies: individual: Sculptor dSph – Local Group – galaxies: stellar content

1 INTRODUCTION

Pulsating variable stars are powerful tools to investigate the evolution of their host galaxy, as they trace the age and the metallicity of the parent population. Most importantly, the coexistence of different types of variable stars provides, thanks to their pulsational properties, independent constraints not only on the star formation history and the chemical evolution, but also on the distance of the system. Indeed,

because pulsations occur at specific evolutionary stages that depend on the stellar mass, variable stars trace the spatial distribution of stellar populations of given ages. Therefore they can be used as markers of spatial trends across the galaxy under examination (e.g., Gallart et al. 2004). Moreover, even the range of pulsational properties among individual stars of a particular type can trace some differences in the age and metallicity of the corresponding population (e.g., Bernard et al. 2008; Martínez-Vázquez et al. 2015).

This paper focuses on the variable-star content of the Local Group dwarf spheroidal (dSph) Sculptor. Sculp-

* E-mail: clara.marvaz@gmail.com (CEM-V)

tor is one of the “classical” Milky Way dSph satellites. After the Magellanic Clouds, it was the first to be discovered along with Fornax (Shapley 1938). Sculptor’s stellar content has been investigated in a large number of papers, using different techniques. Large scale and/or deep photometric surveys provided colour-magnitude diagrams (CMDs) showing an extended horizontal branch (HB, Majewski et al. 1999; Hurley-Keller et al. 1999; Harbeck et al. 2001), and a wide colour spread of the red giant branch first mentioned by Da Costa (1984). While it is well established that Sculptor is composed of a predominantly old population (Monkiewicz et al. 1999; de Boer et al. 2011), it clearly presents some age spread (Tolstoy et al. 2004; de Boer et al. 2012). The chemical enrichment history of Sculptor has been investigated through spectroscopy of its RGB (Tolstoy et al. 2004; Kirby et al. 2009; Starkenburg et al. 2013; Skúladóttir et al. 2015) and HB stars (Clementini et al. 2005), revealing a large range in metallicity, of the order of 1 dex. In Martínez-Vázquez et al. (2015) (hereafter Paper I), based on the pulsational properties of RR Lyrae (RRL) stars, we showed that a similar metallicity spread (~ 0.8 dex) was already in place at an early epoch (>10 Gyr), imprinted in the parent population that we observe today as RRL stars.

The first investigation of the variable-star content in Sculptor dates back to the work by Baade & Hubble (1939) and Thackeray (1950). However it was not until van Aagt (1978) that a conspicuous population of 602 candidate variable stars was discovered and periods for 64 of them were provided.

The most complete catalogue of variable stars (in terms of providing pulsational properties) in Sculptor is that of Kaluzny et al. (1995). They investigated the central region of the Sculptor dSph ($\sim 15' \times 15'$) as a side-program of the OGLE I project. They identified 231 variable stars that were classified as 226 RRL, 3 Anomalous Cepheids (AC), and 2 long period variable (LPV) stars. Their properties are consistent with a metal-poor population ($[\text{Fe}/\text{H}] < -1.7$). A spectroscopic follow-up made by Clementini et al. (2005) confirmed this result through low resolution ($R \approx 800$) spectroscopy of 107 variables using the ΔS method. In particular, they found that the metallicity peaks at $[\text{Fe}/\text{H}] \sim -1.8$.

In Paper I we reported on the detection of a large metallicity spread and spatial gradients within the population of Sculptor’s RRL star population. In this work we present the full catalog of variable stars detected in this galaxy employing the same methodologies as the “Homogeneous Photometry” series (Stetson et al. 1998a; Stetson 2000; Stetson et al. 2003; Stetson 2005; Stetson et al. 2005, 2014). In § 2 we present the extensive data set of 4,404 images used in this analysis. In § 3 we discuss the variable-star detection and classification. We later discuss in detail different families of variable stars: RRL stars (§ 4), AC (§5), SX Phoenicis (SX Phe, § 6), and other groups (peculiar, binaries, long period and probable variable stars, § 7). In § 8 we discuss the properties of the old populations of Sculptor, analysing its RRL stars in detail. A summary of our conclusions (§ 9) closes the paper. We highlight that in the online version of the paper we provide full details on all the variable stars discussed: time series photometry, light curves, mean photometric and pulsational properties and finding charts.

2 PHOTOMETRIC DATA SET

The photometric data set used for this study consists of 5,149 individual CCD images obtained during 21 observing runs between 1987 October and 2011 August (i.e., over nearly 24 years). It covers an area over the sky of ~ 4.7 deg² centred on the Sculptor dSph galaxy. However, only 4,404 images (within ~ 2.5 deg²) were calibrated photometrically, while the area with a significant number of epochs for the variability study is further reduced to ~ 2.0 deg². These data were acquired with a variety of cameras on a number of different telescopes at the European Southern Observatory, Cerro Tololo Interamerican Observatory, and Las Campanas Observatory as detailed in the accompanying Table 1. For each of the observing runs the table specifies the beginning and ending dates of the run (although it is not necessarily true that Sculptor was observed on all the nights during any given run). Table 1 also identifies the telescope and the detector system used for each of the runs, as well as the number of separate exposures obtained in the *B*, *V*, *R*, *I*, and “other” filter passbands. The “multiplex” column indicates the number of individual disjoint CCDs in each instrument. For instance, the ESO/MPI Wide Field Imager used during run, “wfi33”, has eight adjacent CCDs; the six individual exposures obtained during this run produced $6 \times 8 = 48$ separate CCD images that contributed to our overall total of 5,149. However, no individual star was contained in more than six of the 48 images from that run, since the different CCDs map to non-overlapping areas on the sky. Similarly, the SUSI camera on the ESO NTT telescope had two adjacent CCDs, so the 45 individual exposures obtained during run 4, “susi9810,” comprised 90 separate CCD images.

All 5,149 CCD images were processed to produce instrumental magnitudes for individual stars using the DAOPHOT/ALLSTAR/ALLFRAME package of programs (e.g., Stetson 1987, 1994); those which could be were then calibrated using the protocols described by Stetson (2000, 2005). These methods have by now been used in a large number of refereed papers by members of our collaboration, and more elaborate details are not needed here. The few exposures that we have designated as being obtained with “other” filters in Table 1 are not used photometrically here, but they were included in the ALLFRAME reductions to exploit the information they could provide toward the completeness of the star list and the quality of the astrometry.

From two of the observing runs, 7 = wfi36 and 21 = lee1, we inferred at least some magnitudes on the standard Landolt photometric system from observations that were obtained in non-standard filters. In particular, in run 7 (wfi36) 13 exposures were obtained using the standard Wide-Field Imager “B” filter and 13 were obtained with the standard “R” filter. However, an additional nine exposures were obtained using a DDO51 (magnesium hydride) filter (MB#516/16_ESO871, central wavelength 516.5 nm, width 16.2 nm) and another ten were obtained with a Washington *M* filter. (In a quick search on the internet we were unable to locate the filter properties for the ESO/WFI *M* filter, but the defining *M* filter has central wavelength 508.5 nm and width 105.0 nm: Canterna 1976) By simple trial we learned that, allowing for quadratic colour terms in the calibrating transformation equations, we were able to use these filters to predict Landolt-system *V*-band magnitudes with a star-to-

Table 1. Sculptor dSph Observations

Run ID	Run Dates	Telescope	Detector	B	V	R	I	Other	Multiplex	Notes
1 f2	1987 Oct 26	CTIO 0.9m	TI	10	12	–	–	–		
2 ogle	1993 Jun 20-Sep 05	LCO 1.0m	FORD2	–	49	–	–	–		
3 wfi33	1997 Jul 19-23	ESO/MPI 2.2m	WFI	–	3	–	3	–	×8	
4 susi9810	1998 Oct 26-29	ESO NTT 3.6m	SUSI	8	18	–	19	–	×2	
5 susi0008	2000 Aug 07-10	ESO NTT 3.6m	SUSI	7	–	21	–	–	×2	
6 wfi18	2000 Oct 18-22	ESO/MPI 2.2m	WFI	5	3	–	3	1	×8	a
7 wfi36	2002 Aug 30-Sep 03	ESO/MPI 2.2m	WFI	13	19	13	–	–	×8	b
8 wfi34	2002 Oct 12-16	ESO/MPI 2.2m	WFI	20	14	–	–	2	×8	a
9 wfi35	2002 Dec 12-28	ESO/MPI 2.2m	WFI	12	12	–	–	–	×8	
10 wfi31	2003 Sep 18-20	ESO/MPI 2.2m	WFI	2	29	–	30	–	×8	
11 susi0410	2004 Oct 05-09	ESO NTT 3.6m	SUSI	–	–	29	–	–	×2	
12 susi0709	2007 Sep 09-13	ESO NTT 3.6m	SUSI	–	–	92	–	–	×2	
13 susi0711	2007 Nov 07-09	ESO NTT 3.6m	SUSI	–	–	6	–	–	×2	
14 ct08nov	2008 Jul 18-19	CTIO 0.9m	Tek2K3	15	15	–	15	–		
15 B0809	2008 Sep 06-07	CTIO 4.0m	Mosaic2	20	27	–	12	–	×8	
16 B08sep	2008 Sep 24-27	CTIO 4.0m	Mosaic2	98	98	–	14	–	×8	
17 susi0809	2008 Sep 28-29	ESO NTT 3.6m	SUSI	10	–	20	–	–	×2	
18 B0911	2009 Nov 20-24	CTIO 4.0m	Mosaic2	11	39	–	47	–	×8	
19 soar1010	2010 Oct 14	SOAR 4.1m	SOI	–	59	–	–	–	×2	
20 soar1012	2010 Dec 04	SOAR 4.1m	SOI	–	10	–	–	–	×2	
21 lee1	2011 Aug 30	CTIO 4.0m	Mosaic2	3	3	–	–	3	×7	c

Notes. – (a) “Other” filter was U ; these images were not photometrically calibrated. (b) “V” exposures comprised 9 exposures in the DDO 51 filter, plus 10 exposures in the Washington M filter. These were approximately transformed to the Landolt V system. (c) Observations were made in the Strömgren b and y filters, and a Calcium H+K filter. The instrumental b and y magnitudes were approximately transformed to Landolt B and V ; the Ca measurements were not calibrated.

Data credits. – (1) Data contributed by N. B. Suntzeff; (2) Data contributed by A. Udalski –OGLE project–; (3) Program ID unknown, observer unknown; (4) Program ID 62.N-0653(A), observer unknown; (5) Program ID 65.N-0472(A), observer unknown; (6) Program ID 066.B-0615, observer L. Rizzi; (7) Program ID 60.A-9121(A), observer unknown; (8) Program ID 70.B-0696(A), observer unknown; (9) Program ID 70.B-0696(A), observer unknown; (10) Program ID 171.B-0588(C), observer unknown; (11) Program ID 074.B-0456(A), observer unknown; (12) Program ID 079.B-0379(A), observer unknown; (13) Program ID 080.B-0144(A), observer unknown; (14) Observer J. Vasquez, comment “Saha”; (15) Proposal ID 2008B-0143, proposer Saha, observers Saha, Tolstoy, de Boer; (16) Proposal ID 2008B-0206, proposer Bernard, observers Bernard, Walker; (17) Program ID 081.B-0534(A), observer unknown; (18) Proposal ID 2009B-0157, proposer Saha, observers Olsen, de Boer; (19) Proposal “Sculptor Optical Imaging,” proposer Zepf, observers Zepf, Peacock; (20) Proposal ID 2010B-0415, proposer H. Smith, observer unknown; (21) Proposal ID 2011B-0139, proposer J.-W. Lee, observer J.-W. Lee.

star reliability $\sigma \sim 0.05$ mag from the DDO51 magnitudes, and ~ 0.02 mag from the M magnitudes. In our opinion, this precision is good enough to use these observations to help define the variable-star light curves, but we would hesitate to use these in calibrating our best CMD for Sculptor.

Similarly, in the run we have identified as “lee1” (our number 21), the observations were made in the Strömgren b and y filters, and in a Calcium H+K filter. (We were unable to locate the filter characteristics of the Ca filter then in use with the CTIO 4.0m Mosaic Camera, but the filter used on the smaller CTIO telescopes is described as having central wavelength 396.0 nm and width 10.0 nm.) We made no attempt to calibrate the Ca observations photometrically, but we found that with quadratic colour coefficients b could be transformed to B with a star-to-star reliability of 0.03 mag, and y transformed to V with a reliability of 0.02 mag. Again, we feel that these are good enough to employ for the variable-star light curves, but would hesitate to include them in the CMD.

The individual B , V and I measurements for all of the detected variables in the calibrated field of Sculptor are listed in Table 2. They were named with the prefix “scl-CEMV” (which refers to the name of the galaxy and the current work), followed by a number which increases in order of increasing right ascension.

3 VARIABLE STAR IDENTIFICATION AND COLOUR-MAGNITUDE DIAGRAM

We performed the variability search over the full data set, using an updated version of the Welch-Stetson variability index (Welch & Stetson 1993; Stetson 1996) which identifies candidate variable stars on the basis of our multi-band pho-

tometry. From the list of 663 variable candidates, we have identified 574 as actual variable stars (i.e., we can derive periods, amplitudes and mean magnitudes in BVI), 60 as likely variable stars, and 29 as non-variable stars. Figure 1 presents the (V , $B-V$) CMD of Sculptor, with the detected variable stars highlighted. Most of them belong to Sculptor and are located in the instability strip (IS), spanning a wide range of luminosities. In particular, from the brightest to the faintest, we identified four ACs (red circles), three *peculiar* HB variable stars (orange squares, similar variables were detected in Coppola et al. 2013), 536 RRL stars (blue star symbols), five eclipsing binaries (magenta diamonds) and 23 SX Phe stars (green bowties). Moreover, a sample of 31 probable LPV stars (brown triangles) are found near the tip of the Sculptor’s giant branch, plus six more LPVs are spread over the CMD. The three grey open circles mark the position of variable stars that we believe are located along the line of sight of the Sculptor dSph, two of them compatible with being field δ Scuti while the other one is a possible field RRc. Finally, large cyan plusses are 23 stars identified as probable variables. Table 3 reports a summary of the full list of putative variable stars.

We derived pulsational properties for all the variable stars using our BVI -Johnson/Cousins photometry. An initial period search was carried out using a simple string-length algorithm (Stetson et al. 1998b). The intensity-averaged magnitudes and amplitudes of the mono-periodic light curves were obtained by fitting the light curves with a set of templates partly based on the set of Layden et al. (1999) following the method described in Bernard et al. (2009).

Fig. 2 presents the spatial distribution of the detected variable stars (inside of ~ 2 deg²), superimposed on the pho-

Table 2. Photometry of the variable stars in Sculptor dSph.

MHJD ^a	<i>B</i>	σ_B	MHJD ^a	<i>V</i>	σ_V	MHJD ^a	<i>I</i>	σ_I
scl-CEMV001								
54734.613281	19.636	0.011	54734.609375	19.429	0.014	54734.875000	19.460	0.014
54734.656250	19.809	0.017	54734.660156	19.592	0.013	54734.898438	19.475	0.038
54734.718750	20.070	0.026	54734.710938	19.800	0.026	54734.902344	19.403	0.034
54734.750000	20.314	0.311	54734.777344	19.920	0.010	54734.914062	19.806	0.363
54734.773438	20.220	0.010	54734.828125	20.006	0.009	52902.726562	19.512	0.039
54734.824219	20.369	0.011	54735.699219	20.238	0.016	52902.730469	19.450	0.058
54735.707031	20.681	0.014	54736.550781	20.371	0.020	—	—	—
54736.554688	20.794	0.020	54736.742188	19.536	0.010	—	—	—
54736.746094	19.746	0.010	54736.816406	19.732	0.012	—	—	—
54736.824219	20.058	0.012	54736.859375	19.893	0.018	—	—	—
54736.859375	20.150	0.015	54736.894531	19.921	0.020	—	—	—
54736.898438	20.480	0.038	52902.714844	20.041	0.036	—	—	—
—	—	—	52902.722656	20.050	0.025	—	—	—
scl-CEMV002								
54716.597656	20.207	0.028	54716.613281	20.060	0.029	54716.632812	19.757	0.068
54716.601562	20.228	0.013	54716.617188	20.002	0.017	54716.632812	19.841	0.025
54716.609375	20.194	0.011	54716.621094	20.068	0.008	54716.640625	19.807	0.010
54716.613281	20.199	0.013	54716.625000	20.079	0.009	54716.648438	19.761	0.007
54734.566406	20.384	0.010	54716.628906	20.072	0.009	54716.656250	19.791	0.007
54734.613281	20.210	0.009	54734.558594	20.233	0.011	54734.875000	19.842	0.014
54734.656250	20.234	0.009	54734.609375	20.071	0.011	54734.902344	19.832	0.045
54734.773438	20.425	0.010	54734.660156	20.082	0.008	55157.625000	19.880	0.009
54734.824219	20.487	0.012	54734.777344	20.241	0.008	55157.632812	19.888	0.008
54735.554688	20.200	0.012	54734.828125	20.294	0.009	55157.640625	19.924	0.008
54735.605469	20.218	0.011	54735.546875	20.035	0.013	55157.648438	19.942	0.009
54735.652344	20.273	0.011	54735.597656	20.062	0.012	52902.726562	19.904	0.038
54735.707031	20.457	0.011	54735.656250	20.137	0.014	—	—	—
54735.753906	20.483	0.013	54735.699219	20.289	0.013	—	—	—
54736.554688	20.238	0.018	54735.746094	20.277	0.014	—	—	—
54736.601562	20.383	0.014	54736.550781	20.121	0.019	—	—	—
54736.640625	20.517	0.013	54736.601562	20.238	0.015	—	—	—
54736.707031	20.424	0.015	54736.636719	20.293	0.018	—	—	—
54736.746094	20.190	0.012	54736.710938	20.190	0.021	—	—	—
54736.781250	20.205	0.013	54736.742188	20.100	0.016	—	—	—
54736.824219	20.203	0.011	54736.785156	20.029	0.014	—	—	—
54736.859375	20.247	0.013	54736.816406	20.014	0.015	—	—	—
54736.898438	20.334	0.040	54736.859375	20.098	0.017	—	—	—
55159.722656	20.339	0.010	54736.894531	20.239	0.023	—	—	—
55159.726562	20.350	0.009	55157.597656	20.172	0.007	—	—	—
52517.843750	20.263	0.010	55157.613281	20.214	0.007	—	—	—
52517.851562	20.171	0.009	52902.714844	20.318	0.013	—	—	—
52517.855469	20.212	0.010	52518.730469	20.242	0.025	—	—	—
—	—	—	52518.730469	20.213	0.023	—	—	—
—	—	—	52518.734375	20.294	0.023	—	—	—
—	—	—	52518.742188	20.104	0.038	—	—	—
—	—	—	52518.746094	20.185	0.037	—	—	—
—	—	—	52518.753906	20.123	0.039	—	—	—

^a Modified Heliocentric Julian Date of mid-exposure: HJD - 2,400,000

(This table is a portion of its entirety form which will be available in the online journal.)

Table 3. Summary of the detected variable stars inside $\sim 2 \text{ deg}^2$ centred on Sculptor dSph.

Type of variable	Total	Fundamental Mode	First Overtone	Second Overtone	Double Mode
ACTUAL					
AC	4	4	0	0	—
RRL	536	289	197	—	50
SX Phe	23	??	??	??	—
Eclipsing binary	5	—	—	—	—
Field	2 ^a + 1 ^b	—	—	—	—
<i>Peculiar</i> HB	3 ^c	—	—	—	—
LIKELY					
LPV	31 ^d + 6 ^e	—	—	—	—
Probable ^f	23	—	—	—	—

* See § 6 for a detailed discussion of the classification mode.

^a Compatible with being field δ Scuti.^b Compatible with being field RRc.^c In § 7.1, the reader have the explanation of why these stars are considered *peculiar*.^d LPV stars near the tip of the red-giant branch.^e LPV stars out of the tip of the red-giant branch.^f Variable stars for which a proper light curve and a reliable classification is difficult to obtain.

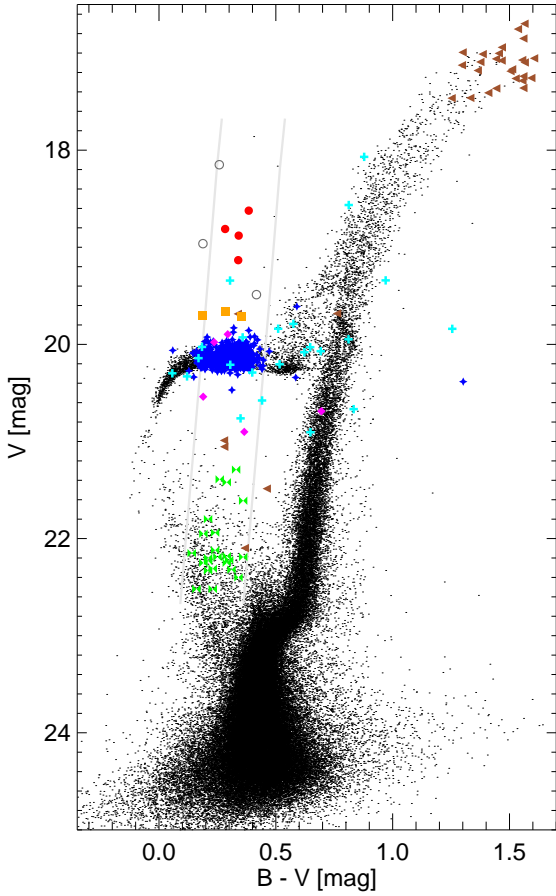


Figure 1. Colour-magnitude diagram of Sculptor with the identification of the all detected variable stars. Green bowtie symbols represent the SX Phoenicis stars. Magenta diamonds are the probable eclipsing binaries. Blue stars are the RR Lyrae stars. Orange square are the three peculiar variables detected in Sculptor. Red circles are anomalous cepheids. Grey open circles are the field variables detected in Sculptor. Brown triangles are the long period variable stars. Large cyan pluses are probable variables. The edges of the Instability Strip are those presented in [Fiorentino et al. \(2006\)](#) extended to low luminosities (light grey lines).

tometrically calibrated part of the field. The solid ellipses mark the core and tidal radii (the latter is only partially visible in the south-west corner). As the present database consists of a large selection of observations collected from different projects, the number of phase points is not constant over the field and increases towards the centre of Sculptor. The dashed ellipse marks the area corresponding to the elliptical radius (equivalent distance along the semi-major axis) of $27.5'$ where we estimate the completeness to be homogeneous (discussed below) in the variable star detection, at least in the magnitude and period range typical of RRL stars. The inner square marks the area covered by the [Kaluzny et al. \(1995\)](#) RRL stars. It is worth mentioning that the covered area is nearly similar to that observed by [van Agt \(1978\)](#). He identified 95 percent of his candidates (602) inside of our current area. However, [van Agt \(1978\)](#)

provided periods only for a few (64). On the other hand, we note that, given the large tidal radius of Sculptor, many RRL stars are likely still to be discovered.

Focusing on the homogeneity of the sample, [Fig. 3](#) shows the number of phase points for each identified RRL star as a function of the elliptical radius for the B , V , and I filters (blue, green, and red dots, respectively). The plot shows that the V band has the largest number of points in the central regions (greater than 170 for elliptical radius $< 5'$ and lower than 100 for elliptical radius $> 5'$ and $< 20'$), while the B observations number above 50 out to $\sim 20'$. The mean number of points in both bands remains above 40 out to $27.5'$. The number of I band points is relatively constant (~ 15) out to the same distance and then slowly declines. Given the large number of independent observing runs and the large time baseline, we are confident that we have a high and relatively homogeneous completeness for detection of RRL stars out to $27.5'$. This is shown as a dashed ellipse in [Fig. 2](#).

4 RR LYRAE STARS

4.1 Classification

Based on the pulsational properties, light curves (LCs), and positions on the CMD, we identify 536 RRL stars. Of these, 390 were flagged by [van Agt \(1978\)](#) as candidate variables (but periods were provided for only 53 of them), and 65 were discovered by [Kaluzny et al. \(1995\)](#); the remaining 81 are new discoveries. [Kaluzny et al. \(1995\)](#) presented the analysis of 226 RRLs, although we show in [§ 4.4](#) that 10 of these are probably not RRLs. Here we provide the pulsation parameters (period, mean magnitude and amplitude) for 320 RRLs for the first time.

We sub-classify the sample of RRL stars as: *i*) 289 RRab, pulsating in the fundamental mode; 20 of them are suspected Blazhko stars, ([Blazhko 1907](#)); *ii*) 197 RRc, pulsating in the first-overtone mode; and *iii*) 50 possible multi-mode RRd stars, pulsating in both modes simultaneously. The classification of the latter was uncertain in some cases due to their relatively noisy or (very) poor light curves.

The LCs of all the RRL stars are presented in [Fig. 4](#) and their basic properties (position, period, amplitude and mean magnitude in B , V and I Johnson/Cousins bands) are detailed in [Table 4](#). The mean (maximum) number of points in the light-curves of the RRL stars are 52, 83, and 21 (115, 182 and 28) respectively in B , V , and I .

[Fig. 1](#) shows that a few RRLs stars appear far from their expected location, presumably due to the poor coverage of the LC causing erroneous mean magnitudes in the different photometric bands. To avoid these outliers, following the procedure of [Paper I](#) we selected those (520) with mean V magnitude within 2.5σ from the average of the population (20.13 mag): these define the *full* sample that will be adopted in the analysis throughout the paper. On the other hand, a more restrictive selection was performed based on the quality of the phase coverage of the photometry over the entire pulsation cycle based on visual inspection of the individual light curves and the period-magnitude diagram, resulting in the sample of 290 RRL stars that we defined as the *clean* sample (tinted background in [Fig. 4](#)). In summary,

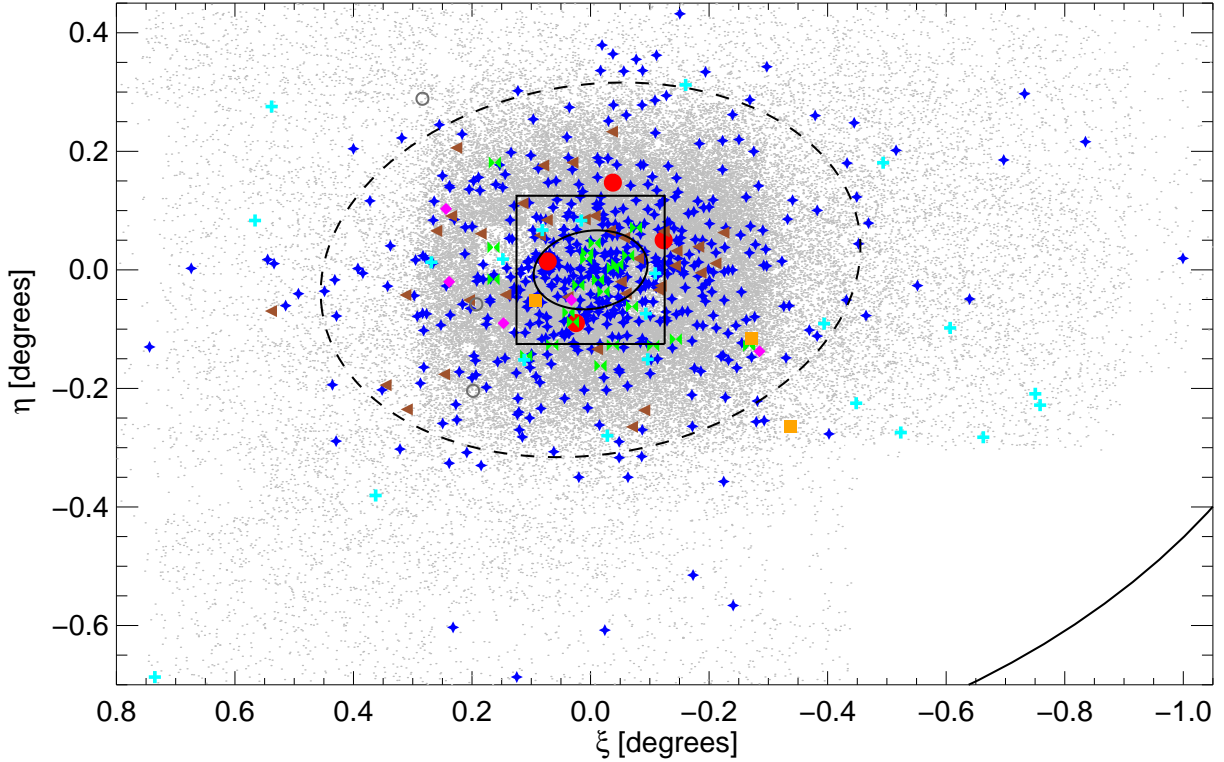


Figure 2. Spatial distribution of the detected variable stars in and around the Sculptor dSph based our current photometry database. Static stars are represented by gray dots. The RRL stars, AC, SX Phe, eclipsing binary, field variable stars, LPV, the three peculiar variables and the probable variable are shown, with the same symbols as in Fig. 1. The innermost ellipse represents the core ($r_c=5.8$ arcmin; Mateo 1998). The outermost ellipse (of which only a small arc appear in the south-west corner) corresponds to the tidal radius ($r_t=76.5$ arcmin; Irwin & Hatzidimitriou 1995). The dashed ellipse is the radius (~ 27.5 arcmin) from which the number of points per light curve of RRL is lower than 40 in the B and V bands. The field of view of the study presented in Kaluzny et al. (1995) ($15' \times 15'$) is represented by the inner square. This field (~ 2 deg 2) covers the area where van Agt (1978) detected the 95 percents of his candidates.

we have identified 276 (167) RRab + 195 (123) RRC + 49 (0) candidate RRd variables in the *full* (*clean*) sample.

4.2 Periods and Amplitudes

Fig. 5 presents a comparison between the amplitudes in the B vs V (upper panel) and V vs I bands (lower panel) for the *clean* sample of RRLs. We used them to perform a linear fit. The red symbols show the outliers rejected with a $3\text{-}\sigma$ clipping selection and not used in the linear fit. The derived values for the amplitude ratios, given by the slopes of the red lines, are 1.229 ± 0.002 (A_B/A_V) and 1.483 ± 0.003 (A_V/A_I). These values are in good agreement both with theoretical predictions (Bono et al. 1997b) and with observations of RRLs in Galactic globular clusters (Di Criscienzo et al. 2011). This supports the accuracy of our derived pulsation properties for Sculptor’s RRL stars.

In Fig. 6, we present the Bailey (period-amplitude)

diagrams (top panels) and the period distributions (bottom panels) for the *full* (left panels) and the *clean* (right panels) samples of RRL stars. Galactic globular clusters (GGCs) with RRLs can be classified into two groups (Oosterhoff 1939), according to the mean period of their RRab stars (Oo-I: 0.55 d, Oo-II: 0.64 d) and RRC stars (Oo-I: 0.32 d, Oo-II: 0.37 d). In the case of Sculptor, we find that the mean periods of the RRab and RRC stars are: $\langle P_{ab} \rangle = 0.602 \pm 0.004$ d ($\sigma = 0.08$) and $\langle P_c \rangle = 0.340 \pm 0.003$ d ($\sigma = 0.04$) for the *full* sample, and $\langle P_{ab} \rangle = 0.609 \pm 0.006$ d ($\sigma = 0.07$) and $\langle P_c \rangle = 0.345 \pm 0.003$ d ($\sigma = 0.03$) for the *clean* sample, thus placing Sculptor squarely in the so-called Oosterhoff gap (see Fig. 5 from Catelan 2009). Therefore, on the basis of the mean period of the RRab (and RRC) stars, Sculptor could be classified as an Oo-intermediate system, as is normal among Local Group dwarf galaxies (Kuehn et al. 2008; Bernard et al. 2009, 2010;

Table 4. Parameters of the RRL stars in Sculptor dSph.

CEMV+2016 name	Original name	Alternative name	RA (J2000)	DEC (J2000)	Period (current)	$\langle B \rangle$	$\langle V \rangle$	$\langle I \rangle$	A_B	A_V	A_I	Q1 ^a	Q2 ^b	Type
scl-CEMV001	V461	—	00 55 21.02	-33 41 01.5	0.420876::	20.150	19.830	19.460	0.900	0.630	0.000	1	X	RRab
scl-CEMV002	—	—	00 56 09.15	-33 29 20.1	0.3059705	20.326	20.163	19.840	0.298	0.254	0.168	0	1	RRc
scl-CEMV005	—	—	00 56 38.94	-33 24 32.4	0.309746	20.260	20.086	19.778	0.494	0.359	0.165	0	1	RRc
scl-CEMV006	—	—	00 56 48.78	-33 31 16.3	0.3321113	20.333	20.117	19.738	0.568	0.479	0.401	0	1	RRc
scl-CEMV008	—	—	00 57 04.83	-33 45 20.6	0.2813182	20.357	20.047	19.570	0.881	0.576	0.485	2	0	RRc
scl-CEMV010	—	—	00 57 30.30	-33 44 01.7	0.4056391	20.252	19.982	19.637	0.632	0.466	0.265	0	1	RRc
scl-CEMV012	V483	—	00 57 41.04	-33 30 21.9	0.3702771	20.307	20.037	19.619	0.740	0.613	0.424	0	1	RRc
scl-CEMV014	V348	—	00 57 54.19	-33 37 43.5	0.3837578	20.405	20.131	19.676	0.606	0.469	0.276	0	1	RRc
scl-CEMV015	V301	—	00 57 55.25	-33 47 05.1	0.659572	20.418	20.077	19.539	1.075	0.886	0.451	0	1	RRab
scl-CEMV016	V302	—	00 57 59.11	-33 39 50.6	0.3955858	20.362	20.101	19.609	0.515	0.442	0.336	0	1	RRc
scl-CEMV018	V363	—	00 57 59.90	-33 35 06.7	0.5787198	20.400	20.110	19.586	1.366	1.187	0.700	0	0	RRab
scl-CEMV019	V535	—	00 58 01.34	-33 27 36.1	0.3545968	20.347	20.117	19.749	0.734	0.582	0.337	0	1	RRc
scl-CEMV020	V482	—	00 58 04.91	-33 31 39.9	0.3621706	20.397	20.151	19.724	0.591	0.499	0.287	0	1	RRc
scl-CEMV021	V520	—	00 58 04.83	-33 45 33.3	0.6721255	20.537	20.152	19.546	0.726	0.645	0.336	0	1	RRab
scl-CEMV022	V326	—	00 58 12.91	-33 59 05.8	0.5797025	20.414	20.109	19.579	1.210	0.985	0.572	0	1	RRab
scl-CEMV024	V334	—	00 58 18.89	-33 49 10.9	0.537455	20.578	20.254	19.831	0.793	0.644	0.399	3	0	RRab
scl-CEMV025	V456	—	00 58 19.14	-33 36 29.6	0.5928154	20.468	20.136	19.616	1.202	0.910	0.585	0	1	RRab
scl-CEMV026	—	—	00 58 20.51	-33 26 54.2	0.3934555	20.370	20.120	19.649	0.535	0.418	0.325	0	1	RRc
scl-CEMV027	—	—	00 58 22.85	-33 48 34.8	0.3700876	20.465	20.194	19.742	0.657	0.499	0.368	2	0	RRc
scl-CEMV028	—	—	00 58 31.22	-33 35 27.9	0.3203025	20.388	20.184	19.824	0.705	0.567	0.238	0	1	RRc
scl-CEMV030	—	—	00 58 32.76	-33 46 08.8	0.6897029	20.408	20.036	19.468	0.971	0.725	0.388	0	1	RRab
scl-CEMV031	V399	—	00 58 33.54	-33 37 23.7	0.5836000	20.519	20.173	19.606	0.652	0.548	0.306	0	1	RRab
scl-CEMV032	V336	—	00 58 34.15	-33 51 25.4	0.5630753	20.574	20.215	19.692	1.101	0.980	0.637	0	1	RRab
scl-CEMV033	V431	—	00 58 35.20	-33 46 12.2	0.3609695	20.382	20.138	19.679	0.649	0.522	0.259	0	1	RRc
scl-CEMV034	V303	—	00 58 36.35	-33 41 37.3	0.3495360	20.442	20.201	19.803	0.612	0.517	0.325	0	1	RRc
scl-CEMV035	V250	—	00 58 43.74	-33 42 06.1	0.6803114	20.415	20.074	19.474	1.108	0.852	0.577	0	1	RRab
scl-CEMV036	—	—	00 58 43.85	-33 21 58.1	0.337761	20.279	20.111	19.754	0.594	0.530	0.269	0	1	RRc
scl-CEMV037	—	—	00 58 44.07	-33 40 26.2	0.6682190	20.344	20.015	19.432	1.251	1.060	0.714	0	1	RRab
scl-CEMV038	V246	—	00 58 44.60	-33 57 46.3	0.6700931	20.357	20.043	19.547	1.163	0.961	0.608	0	1	RRab
scl-CEMV039	V556	—	00 58 45.04	-33 42 03.1	0.525160	20.505	20.215	19.900	1.167	1.029	0.460	3	0	RRab
scl-CEMV040	—	—	00 58 45.51	-33 38 32.8	0.3107837	20.469	20.239	19.848	0.698	0.533	0.325	3	0	RRc
scl-CEMV042	—	—	00 58 47.73	-33 34 01.5	0.3027722	20.412	20.194	19.839	0.689	0.568	0.343	0	1	RRc
scl-CEMV043	—	—	00 58 48.10	-33 55 48.6	0.2857029	20.403	20.216	19.866	0.259	0.242	0.192	2	0	RRc
scl-CEMV044	V485	—	00 58 48.46	-33 57 55.5	0.3550839	20.487	20.240	19.831	0.555	0.448	0.211	0	1	RRc
scl-CEMV045	—	—	00 58 49.27	-33 39 58.7	0.638994	20.447	20.122	19.630	0.637	0.618	0.424	2	0	RRab
scl-CEMV046	V135	—	00 58 49.35	-33 47 17.0	0.5100380	20.466	20.186	19.786	1.494	1.262	0.723	0	1	RRab
scl-CEMV047	V534	—	00 58 50.28	-33 30 31.4	0.4927699	20.551	20.271	19.790	1.320	1.030	0.715	2	0	RRab
scl-CEMV049	V496	—	00 58 50.83	-33 51 21.2	0.3651721	20.168	19.972	19.585	0.385	0.313	0.255	3	0	RRc
scl-CEMV050	V460	—	00 58 51.56	-33 38 06.7	0.3630319	20.428	20.175	19.762	0.529	0.442	0.169	2	0	RRd

^a Q1 is a parameter associated with quality of the light curve: 0-good, 1-poor quality, 2-noisy, 3-outliers, 4-blended, 5-Blazhko effect.

^b Q2 is a parameter related with the coverage of the light curve: 0-not well sampled and/or too noisy (*full* RRLs sample), 1-well sampled and not too noisy (*clean* RRLs sample). In the case of the 16 outliers, they are pointed out by an “X”.

Full version are available as Supporting Information with the online version of the paper.

Garofalo et al. 2013; Stetson et al. 2014; Cusano et al. 2015; Ordoñez & Sarajedini 2016).

Another tool used to classify GGCs in Oo-type is the Bailey diagram. Oo-I and Oo-II clusters commonly follow the two distinct curves shown in Fig. 6 (top panels) and defined in Cacciari et al. (2005). The RRLs in Sculptor present a significantly wider distribution than either Oo-class. In fact, for each given amplitude stars cover a large period range around both Oo-lines, with a minor fraction populating the intermediate region. It is clear that an Oo-intermediate classification does not necessarily mean that stars are predominantly *between* the Oo-I and Oo-II loci; the distribution also extends to and beyond those loci. Therefore, a classification based only on the mean periods for RRab-type (and/or RRc-type) stars is clearly insufficient to characterize the range of properties among the RRL stars in Sculptor.

As we demonstrated in Paper I, the RRL stars show a spread in V magnitude of ~ 0.35 mag, significantly larger than the typical uncertainties in the mean magnitude ($\sigma=0.03$ mag), and larger than the spread expected from the simple ageing of a mono-metallic population. We also show that the vast majority of the RRLs span a significant metallicity spread of ~ 0.8 dex, bracketed between ~ -2.3 and ~ -1.5 dex. When splitting the sample of RRLs

at $\langle V_{RRL} \rangle = 20.155$ mag, thus defining a *bright* (Bt) and a *faint* (Ft) sample, the spread in metallicity is reflected in the two groups. In Martínez-Vázquez et al. (2016, Paper II), we show that the Bt sample is, on average, more metal-poor ($\langle [Fe/H]_{Bt} \rangle = -2.03$) than the Ft one ($\langle [Fe/H]_{Ft} \rangle = -1.74$).

The Bailey diagram (Fig. 6) shows the Bt and Ft samples with blue and orange symbols, respectively. Interestingly, stars selected in the CMD are clearly separated in the Bailey diagram as well: Bt, metal-poor RRL stars are closer to the Oo-II sequence, while Ft, more metal-rich RRL stars follow a distribution similar to an Oo-I system. This is also reflected in the mean periods of the Bt and Ft groups, which are similar to those defining the OoII and OoI systems, respectively (see Table 5). This supports the conclusion that in complicated systems such as Sculptor, characterized by an important chemical evolution at an early epoch, the Oosterhoff classification must be treated cautiously, and that the mean period alone does not provide a full characterisation of the target stellar system.

Fig. 6 also provides constraints on the old galaxy stellar population:

(i) The fraction of RRc stars in the *full* sample, $f_c = \frac{N_c}{N_{ab} + N_c} = 0.41$ ($f_c = 0.42$ for the *clean* sample of RRLs) in agreement with Kaluzny et al. 1995, is relatively higher than in the rest of the other dSph galaxies (see Table 6 of

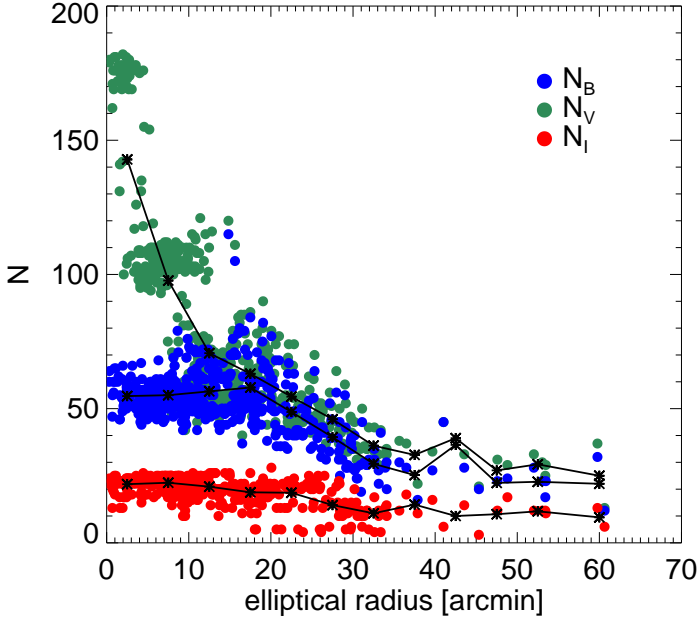


Figure 3. Number of phase points for each identified RRL star as a function of the elliptical radius for the B (blue dots), V (green dots), and I (red dots) filters. Asterisks represent the mean value of each of them every $5'$ (with exception of the last one that covers $10'$, from $55'$ to $65'$).

Table 5. Mean period of the Bt and Ft groups for both *full* and *clean* RRL samples.

	$\langle P_{ab} \rangle$	$\langle P_c \rangle$
FAINT (Ft)		
<i>full</i>	0.560 ± 0.004 d ($\sigma=0.05$)	0.325 ± 0.007 d ($\sigma=0.03$)
<i>clean</i>	0.560 ± 0.006 d ($\sigma=0.05$)	0.332 ± 0.003 d ($\sigma=0.03$)
BRIGHT (Bt)		
<i>full</i>	0.639 ± 0.006 d ($\sigma=0.08$)	0.356 ± 0.006 d ($\sigma=0.03$)
<i>clean</i>	0.647 ± 0.007 d ($\sigma=0.07$)	0.362 ± 0.004 d ($\sigma=0.03$)

Stetson et al. 2014): it is almost twice the f_c obtained in other dSphs. This may be linked to the HB morphology, which has a strong blue component in Sculptor, which may in turn be linked to the details of its early star-formation history.

(ii) The shortest period found for the RRab stars is 0.48230141 days (with $A_V=1.280$ mag, star: scl-CEMV397). The lack of High Amplitude Short Period fundamental RRL stars (HASP; $A_V \gtrsim 0.75$ mag, $P \leq 0.48$ ($\log P \leq -0.32$) Fiorentino et al. 2015a) suggests that Sculptor does not host a significant metal-rich ($[\text{Fe}/\text{H}] \gtrsim -1.5$) old stellar population, as has been confirmed in our analysis of Paper I.

4.3 Distance to Sculptor from the RRL stars

In Paper I we estimated the true distance modulus from the *full* sample as well as the *clean* sample of RRLs. The distance estimates to Sculptor were derived using the three different subsamples (RRab, RRc, and RRab+RRc fundamentalized). The use of three photometric bands and two period-Wesenheit relations (PWR) in V , $B-V$, and V , $B-I$ (these

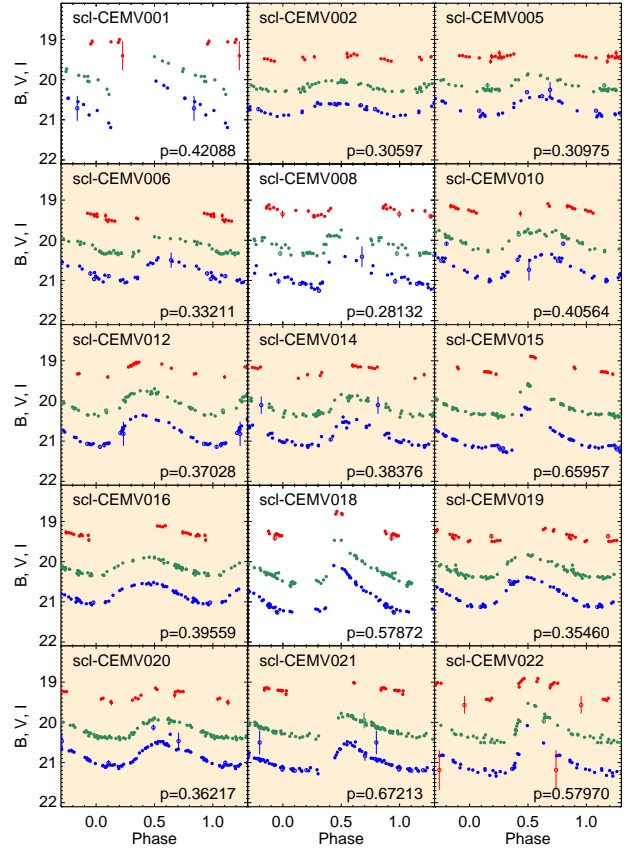


Figure 4. Sample of light curves of the RRL stars in the B (blue), V (green) and I (red) bands, phased with the period in days given in the lower right-hand corner of each panel. The name of the variable is given in the left-hand corner of each panel. Open symbols show the bad data points, i.e., with errors larger than 3σ above the mean error of a given star; these were not used in the calculation of the period and mean magnitudes. For clarity, the B and I light curves have been shifted by 0.4 mag down and upward, respectively. Tinted backgrounds mark those RRL stars classified as members of the *clean* sample. All light curves are available as Supporting Information with the online version of the paper.

are reddening-free and are only minimally affected by the metal content, Marconi et al. 2015) allowed us to provide a very accurate distance. Table 3 in Paper I summarizes the individual distance moduli obtained applying different calibrations¹. The errors on individual distance moduli are never larger than 0.02_{sys} and 0.09_{ran} . Finally, we adopted a mean true distance modulus (μ) of 19.62 mag with $\sigma=0.04$ (see § 4 of Paper I for more details). This estimate is in good agreement with values based on other reliable indicators (Rizzi 2002; Pietrzynski et al. 2008).

¹ It is worth mentioning that Ft and Bt samples produce similar distance moduli.

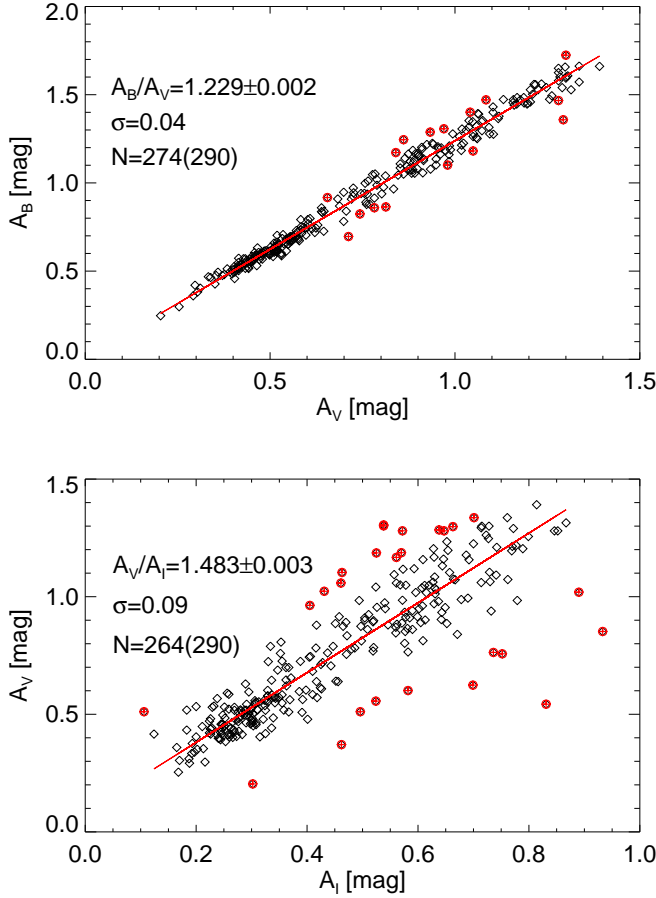


Figure 5. B -amplitude versus V -amplitude diagram (top) and V -amplitude versus I -amplitude diagram (bottom). The slopes obtained here are in good agreement with those predicted for the RRLs of the Galactic GCs (Di Criscienzo et al. 2011). In both cases, the linear fit was performed through the *clean* sample of RRLs in Sculptor, applying least squares fit and a 3σ clipping.

4.4 Comparison with the Kaluzny catalogue

Kaluzny et al. (1995) published a list of 226 RRL stars covering the central $15' \times 15'$ of Sculptor. We matched the two catalogues in order to check the consistency of the derived pulsational properties. 216 of Kaluzny’s RRL stars are included in our sample. It is worth mentioning that the work of Kaluzny et al. (1995) includes 226 sources, but we realized that: *i*) 5 of these stars were duplicated (K1926=K406, K2558=K2058, K2559=K2059, K3345=K1439, K4233=K2423); *ii*) one (K403) is not variable in our photometry; *iii*) the variability of K5081 is not certain based on our data; *iv*) one more star is possibly misclassified, and we catalogue it as probable eclipsing binary (K3710, Clementini et al. 2005); *v*) for two of the Kaluzny’s stars (K737, K4780) we are not able to derive a reliable period. The 3 AC (K3302-V25, K734-V119, and K5689) and the 2 LPV (K274 and K687) analysed in Kaluzny et al. (1995) were also found in our catalogue so, in total, we matched 224 variable stars (216 RRL + 3 AC + 2 LPV + 1 eclipsing binary + 2 probable variable stars).

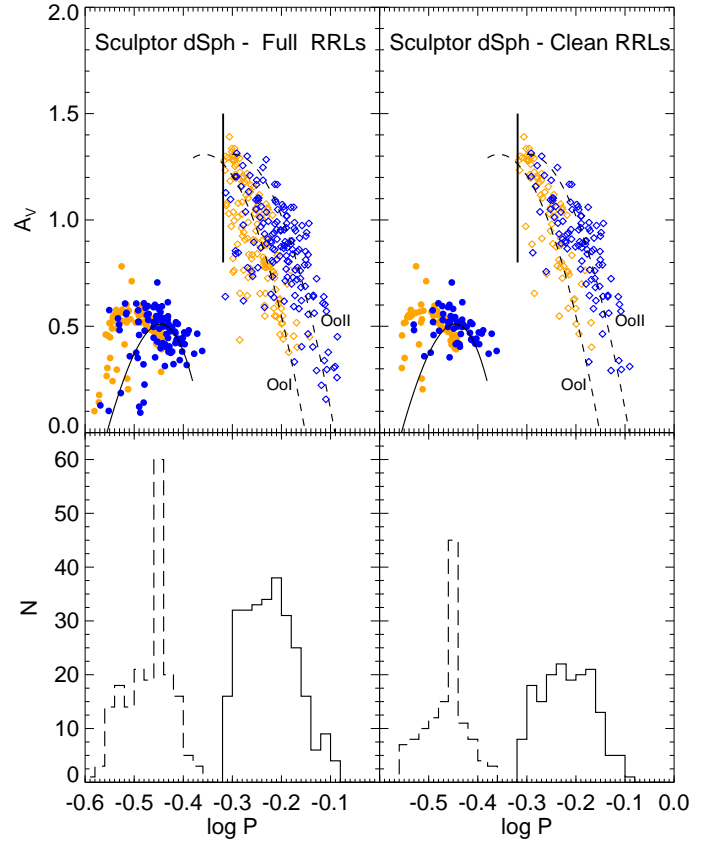


Figure 6. Top. Period-amplitude or Bailey diagrams for the *full* (left-hand panels) and for the *clean* (right-hand panels) samples of RR Lyrae stars in Sculptor. Open diamonds and filled circles represent RRab and RRc, respectively. The dashed lines are the relations for RRab stars in OoI and OoII clusters obtained by Cacciari et al. (2005) for the M3 RRab variables. The solid curve is derived from the M22 (OoII cluster) RRc variable study by Kunder et al. (2013). Black vertical lines mark the HASP limit defined by Fiorentino et al. (2015a). Bottom. Period histograms for those RR Lyrae stars shown in the top panels. RRab and RRc are shown as histograms with solid and dashed lines, respectively. For the sake of clarity, RRd stars are not plotted as their periods are less certain.

The individual and global properties they found are in good agreement with the values we redetermined. In particular, 90 percent of the stars matched have the same periods in both catalogues, within 0.001 days. The global properties are also in good agreement, despite the fact that the two surveys cover a different fraction of Sculptor’s main body. Kaluzny et al. (1995) found that the mean period of the fundamental pulsators and the frequency of first overtones are, respectively, $\langle P_{ab} \rangle = 0.585$ d, $\langle P_c \rangle = 0.338$ d, and $f_c = 0.40$. In this work, the mean periods of the 289 RRab and 197 RRc are $\langle P_{ab} \rangle = 0.602 \pm 0.004$ d ($\sigma = 0.08$), and $\langle P_c \rangle = 0.340 \pm 0.003$ d ($\sigma = 0.04$), respectively. The fraction of RRc variables is equal to $f_c = 0.41$ and becomes 0.46 if we also include the RRd, i.e., $f_{cd} = 0.46$. It has to be stressed

that roughly 2/3 of the OGLE images are included in our sample. The few outliers with discrepant periods in the two studies can be ascribed to an aliasing problem, which is more likely solved by our larger database. Nevertheless, the overall excellent agreement is further independent proof of the quality of the OGLE data and observing strategy, even with a limited number of phase points as in this case.

5 ANOMALOUS CEPHEID STARS

We confirm the existence of 4 Anomalous Cepheids (ACs) in Sculptor, as previously found by [Smith & Stryker \(1986\)](#) and [Kaluzny et al. \(1995\)](#). In Table 6 we summarize the properties of these stars. Two of them (scl-CEMV284 and scl-CEMV388) were discovered by [Baade & Hubble \(1939\)](#) and analysed for the first time by [Swope \(1968\)](#), obtaining periods of 0.926 and 1.346 days, respectively. Another (scl-CEMV160) was discovered by [Thackeray \(1950\)](#), who obtained a period of 1.15 days. All three of these variables were included in the [van Agt \(1978\)](#) catalogue, with similar periods. The fourth AC, scl-CEMV447, was discovered and classified as such by [Kaluzny et al. \(1995\)](#), with a period of 0.85541 days. These previous determinations of the periods for the four ACs are in good agreement with those presented here (see the sixth column in Table 6).

ACs can form through two different channels ([Bono et al. 1997a](#); [Cassisi & Salaris 2013](#)). They can be the progeny of coalesced binary stars, thus evolved blue straggler stars (BSS) tracing the old population ([Renzini et al. 1977](#); [Hirshfeld 1980](#); [Sills et al. 2009](#)). Alternatively, they can be a life stage of metal-poor ($Z < 0.0006$, [Fiorentino et al. 2006](#)), single stars with mass between ~ 1.2 and $\sim 2.2 M_{\odot}$ and age between 1 and 6 Gyr ([Demarque & Hirshfeld 1975](#); [Norris & Zinn 1975](#); [Castellani & degl'Innocenti 1995](#); [Caputo et al. 1999](#)). Given the predominantly old stellar population of Sculptor ([de Boer et al. 2012](#)), it is unlikely that ACs proceed from such a young, elusive population (if any), in agreement also with the analysis of the BSS population ([Mapelli et al. 2009](#)) which excludes the occurrence of such young stars in Sculptor.

The classification of the pulsation mode of ACs is not trivial and cannot be easily determined from the morphology of the light curves (Fig. 7) or from the period-amplitude diagram alone. Theoretical predictions indicate that for the same luminosity and colour, first-overtone (FO) pulsators are less massive than fundamental (F) pulsators. Therefore, determining the correct pulsational mode is important for obtaining a reliable mass estimate. To distinguish between F and FO pulsators we follow two approaches. First, the different pulsation modes follow different period-luminosity relations – which are also different from those of classical and type II cepheids. Their location in the PL diagram can therefore be used to constrain their pulsation mode (see, e.g., [Bernard et al. 2013](#)). We find that all four ACs in Sculptor fall squarely on the sequence corresponding to the fundamental mode ACs. The second approach has been presented in [Fiorentino & Monelli \(2012\)](#), and is based on the method described in [Marconi et al. \(2004\)](#). It is known that ACs obey well-defined mass-dependent period-luminosity-amplitude (MPLA) and period-luminosity-colour (MPLC) relations ([Marconi et al. 2004](#)):

$$\log \frac{M_{MPLA,F}}{M_{\odot}} = (0.01 - 0.188 \cdot A_V - \log P - 0.41 \cdot M_V) / 0.77 \quad (1)$$

$$\log \frac{M_{MPLC,F}}{M_{\odot}} = -(M_V + 1.56 + 2.85 \cdot \log P - 3.51 \cdot (M_B - M_V)) / 1.88 \quad (2)$$

$$\log \frac{M_{MPLC,FO}}{M_{\odot}} = -(M_V + 1.92 + 2.90 \cdot \log P - 3.43 \cdot (M_B - M_V)) / 1.82 \quad (3)$$

However, the MPLA relation is only valid for F pulsators, whereas MPLC relations exist for both pulsation modes.

In order to assign a pulsation mode and a mass to each AC, we proceed as follows. We first estimate the mass using both the MPLA and MPLC relations for F pulsators. Then, when these two values agree with each other within $2\text{-}\sigma$, we classify the star as F mode and take the mean mass as the true value. If instead the two mass estimates are not consistent, we assume that the star is a FO pulsator and we use the corresponding MPLC relation for the mass estimation. This method confirms independently that all ACs are F pulsators (see Table 7).

[Smith & Stryker \(1986\)](#) provided a mass value for two Sculptor ACs: scl-CEMV284 ($2.0^{+1.4}_{-0.8} M_{\odot}$) and scl-CEMV388 ($0.6^{+0.4}_{-0.2} M_{\odot}$) from a linear pulsation theory assuming that they pulsate in the F mode with a pulsational constant of $Q=0.0034$ ([Wallerstein & Cox 1984](#)). The first value is in agreement within the errors with our estimate, but the second one is different at the $3\text{-}\sigma$ level. Nevertheless, as [Smith & Stryker \(1986\)](#) noted, both their mass estimates have substantial uncertainties due to their photometry, and our improved data make us more confident in our determinations.

Fig 8 is a zoom-in of the CMD on the region of AC stars that shows a comparison of theoretical evolutionary tracks for different masses ($1.5 - 3.0 M_{\odot}$) and $[\text{Fe}/\text{H}]$ (-2.0 and -1.8). The adopted stellar models have been retrieved from the BaSTI library ([Pietrinferni et al. 2004](#)) or—when not available in the database—have been computed for this specific project using a theoretical framework fully consistent with the BaSTI assumptions. In more detail, the models shown in Fig. 8 are based on a scaled-solar heavy element mixture, assume a canonical (no overshooting) physical framework, and a mass loss efficiency on the RGB with the free parameter η entering in the [Reimers \(1975\)](#) law set to 0.4. The models were shifted using the distance modulus $\mu=19.62$ mag ([Paper I](#)) and foreground reddening $E(B-V)=0.018$ mag ([Pietrzynski et al. 2008](#)), and assuming the standard extinction law from [Cardelli et al. \(1989\)](#). The blue lines show the zero-age helium-burning (ZAHeB) loci for stars with masses from ~ 1 to $3 M_{\odot}$. Green dashed and black solid lines correspond to the core He-burning evolutionary tracks for stellar models igniting triple- α nuclear reactions at the tip of the RGB under conditions of partial electron degeneracy (initial mass lower than $\sim 2.0 M_{\odot}$) and no-electron degeneracy, respectively (see [Cassisi & Salaris 2013](#) for a detailed review on this topic). The termination of the core He-burning stage (central He abundance equal to 10 percent of the initial value) is marked as green and

Table 6. Parameters of the AC stars in Sculptor dSph.

CEMV+2016 name	Original name	Alternative name	RA (J2000)	DEC (J2000)	Period (current)	$\langle B \rangle$	$\langle V \rangle$	$\langle I \rangle$	A_B	A_V	A_I	Q1	Q2	Type
scl-CEMV160	V119	K734	00 59 33.93	-33 39 31.0	1.1577836	19.221	18.880	18.284	0.703	0.647	0.343	0	1	F
scl-CEMV284	V25	—	00 59 58.53	-33 33 42.2	0.9255408	19.095	18.812	18.379	1.600	1.195	0.737	0	1	F
scl-CEMV388	V26	K3302	01 00 16.64	-33 47 57.4	1.3460368	19.007	18.623	18.097	1.045	0.863	0.536	0	1	F
scl-CEMV447	K5689	—	01 00 30.32	-33 41 42.5	0.8554217	19.472	19.133	18.617	0.941	0.715	0.381	2	0	F

See the caption of Table 4 for a description of the Q1 and Q2 parameters.

Table 7. Parameters of the AC stars in Sculptor dSph.

CEMV+2016 name	$M_{MPLA,FU}$ M_{\odot}	$M_{MPLC,FU}$ M_{\odot}	$M_{MPLC,FO}$ M_{\odot}	MODE _{mass}	$\langle M \rangle^*$ M_{\odot}
scl-CEMV160	1.56 ± 0.18	1.23 ± 0.06	0.77 ± 0.04	F	1.40 ± 0.19
scl-CEMV284	1.68 ± 0.19	1.50 ± 0.07	0.94 ± 0.04	F	1.59 ± 0.21
scl-CEMV388	1.57 ± 0.18	1.65 ± 0.08	1.02 ± 0.05	F	1.61 ± 0.20
scl-CEMV447	1.64 ± 0.19	1.45 ± 0.07	0.90 ± 0.04	F	1.54 ± 0.20

*The final mean value is the mean of the fundamental estimates.

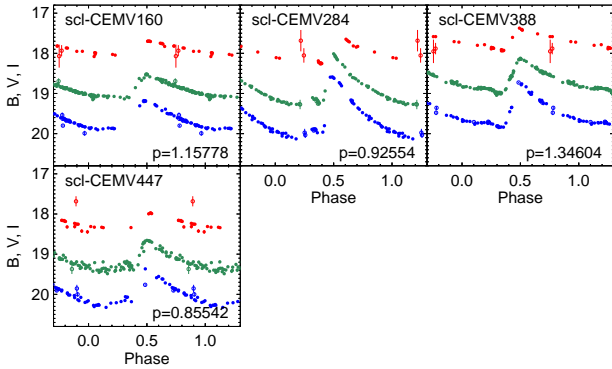


Figure 7. Sample of light curves of the AC stars in the B (blue), V (green) and I (red) bands, phased with the period in days given in the lower right-hand corner of each panel. The name of the variable is given in the left-hand corner of each panel. Open symbols show the bad data points, i.e., with discrepancies larger than 3σ above the standard error of a given star; these were not used in the calculation of the period and mean magnitudes. For clarity, the B and I light curves have been shifted by 0.4 mag down- and upward, respectively.

black stars, respectively. The gray lines correspond to the boundaries of the instability strip (Fiorentino et al. 2006).

The left panel of Fig. 8 shows that a metallicity of $[\text{Fe}/\text{H}]=-2.0$ provides a good match between the location of three of the observed stars and the tracks with mass value in the range $1.60-1.80 M_{\odot}$. These masses are in good agreement, within the errors, with the mean mass estimated above: $\langle M_{AC} \rangle = 1.54 M_{\odot}$ ($\sigma_{sys} = 0.20 M_{\odot}$, $\sigma_{ran} = 0.08 M_{\odot}$). However, the brightest AC is ~ 0.1 mag brighter than expected at this metallicity. An increase in metallicity by 0.2 dex (right panel) provides a good fit of all four stars, but implies slightly larger stellar masses of $\sim 1.90 M_{\odot}$ that is in agreement, for the adopted theoretical scenario, within 2σ .

These two low metallicities are in agreement with previous estimates by Smith & Stryker (1986), who gave a mean value close to $[\text{Fe}/\text{H}]=-1.9$ ($\sigma = 0.3$ dex)² as the mean of

three out of the four ACs (scl-CEMV284, scl-CEMV388 and scl-CEMV160).

6 SX PHOENICIS STARS

Fig. 9 shows the light curves of the 23 variable stars identified in the relatively faint part of the CMD of Sculptor, where the IS crosses the MS and the sub-giant branch for masses typically larger than $1 M_{\odot}$ (see Fig. 1). In this region, variable stars are characterized by short periods (from minutes to a few hours) and low amplitudes (a few tenths of a magnitude). They typically present several pulsation modes simultaneously, both radial and non-radial (Santolamazza et al. 2001; Poretti et al. 2008). These properties makes them elusive targets in external galaxies, as the intrinsic faint brightness makes them difficult to detect, given that the long exposure times required to have good measurements conflict with their short periods. Commonly, these variable stars are classified as δ Scuti when they are population I (young and more metal-rich stars), or SX Phoenicis (SX Phe) when they are population II metal-poor counterparts. The latter are typically observed in GCs, and they are associated with the BSS that, leaving the MS, cross the IS above the main-sequence turnoff of the cluster population. SX Phe stars are important because their pulsational properties allow us to derive their distances (McNamara 2011) and structural parameters such as the BSS mass (Fiorentino et al. 2014, 2015b), which is a key ingredient in deriving the dynamical friction in globular clusters (Ferraro et al. 2012).

In the case of dwarf galaxies the situation is more complicated. On the one hand, dwarf galaxies that are composed of old populations only (> 10 Gyr, or *fast* systems according to the nomenclature introduced by Gallart et al. 2015) appear similar to GCs: the colour of the main-sequence turnoff (MSTO) stars is redder than the red edge of the IS. Therefore, only BSS stars (bluer and brighter than the MSTO stars) can cross the IS at this magnitude level when moving red-ward after central H exhaustion. On the other hand, *slow* dwarf galaxies characterized by star formation at all epochs can host a mix of different variable stars in this region of the

metallicities for the ACs through an adaptation of the ΔS method for RRLs.

² Smith & Stryker (1986) used the ΔS parameter to measure the

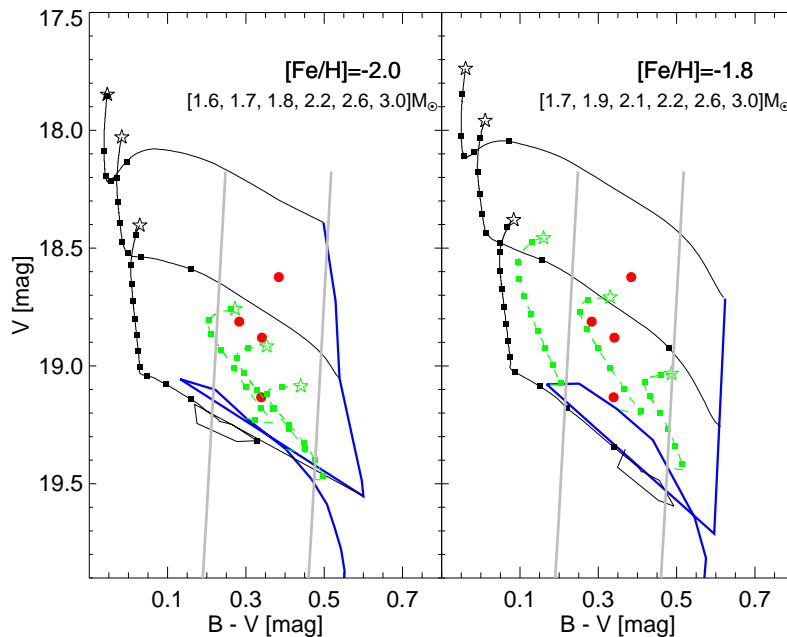


Figure 8. Optical ($B-V$, V) CMDs of Sculptor, zoom-in on AC stars, where theoretical predictions from BaSTI library (Pietrinferni et al. 2004) are over-plotted. Solid grey lines represent the theoretical instability strip (Fiorentino et al. 2006). The red dots indicate the 4 ACs found in Sculptor. The blue lines show the zero-age helium-burning (ZAHeB) loci for stars with masses in the range between ~ 1.0 and $3.0 M_{\odot}$. Evolutionary tracks for AC stars for the labelled masses are shown for different metallicities: $[\text{Fe}/\text{H}]=-2.0$ (left), $[\text{Fe}/\text{H}]=-1.8$ (right). Green and black lines indicate models that ignite helium in the core in degenerate and non-degenerate conditions, respectively. These stellar tracks represent the path from the ZAHeB to the central helium exhaustion (10 percent of the initial abundance), indicated by an open star symbol, at different stellar masses. For the theoretical analysis we used scaled-solar evolutionary models, with a fixed $\Delta Y/\Delta Z=1.4$ and a primordial $Y=0.245$, assumed a distance modulus of $\mu=19.62$ mag (Paper I) and a reddening of 0.018 mag (McConnachie 2012).

CMD (see the case of Carina, Coppola et al. 2015 and the Large Magellanic Cloud, Poleski et al. 2010). Given the lack of evidence for the presence of a young population in Sculptor (see § 5), we assume here that these are the progeny of coalesced binaries stars, and therefore SX Phe.

SX Phe stars of different pulsational modes do not show a clear separation in the period-amplitude diagram. However, they do follow a period-luminosity relation (McNamara 2000; Petersen & Christensen-Dalsgaard 1999; Fiorentino et al. 2014).

Considering the above evidence and taking advantage of the models/relations developed in Fiorentino et al. (2015b), we obtain the theoretical pulsation parameters for the 23 SX Phe stars discovered for the first time in Sculptor (see Table 8). First, we used the predicted PL relations in the B and V bands to perform a detailed mode identification, assuming the distance modulus derived in Paper I and reddening from Pietrzynski et al. (2008). Pulsation modes can best be identified using the theoretical predictions in the B -band PL planes (see Table 3 in Fiorentino et al. 2015b) because the B -band is the least noisy for this kind of star. We considered the relation for metallicities $Z=0.001$ and $Z=0.0001$. The pulsation modes (F-fundamental-, FO-first overtone-, SO-second overtone-, and TO-third overtone-) have been determined according to the proximity to a PL relation in the M_B -period plane.

Figure 10 shows the absolute B -band and V -band PL relations. The latter is used as a consistency

check of the pulsation mode chosen. For the metallicity $Z=0.001$ ($Z=0.0001$)—solid (dashed) lines—we assign the following modes: 0(0) F, 16(17) FO, 6(5) SO, 0(0) TO. Both metallicities provide similar pulsation modes for the population of SX Phe stars. Furthermore, we note that the spread around the PL relations with such a classification is very small, i.e., $\sigma_{FO}=0.02$ mag and $\sigma_{SO}=0.05$ mag. However, we note that mode classification in this type of variable star is still uncertain. For example, the empirical relations of Pych et al. (2001), with slope and zero-point similar to those from the theoretical models of Fiorentino et al. (2015b), provide the same modes. On the other hand, the empirical relations such as, e.g., McNamara (2011) (their eq. 5a and 5b) instead suggest that 15(13) are F and 5(5) are FO; this is due to the relations having similar slopes but a zero-point offset of ~ 0.3 . Further studies of SX Phe stars targeting nearby galaxies (as, e.g., Coppola et al. 2015 in Carina) are warranted in order to help to clarify the situation.

Once the pulsation mode is adopted for each SX Phe star, we can use the Mass-Period-Luminosity-Metallicity relations (see Table 6 in Fiorentino et al. 2015b) for each selected pulsation mode to estimate the masses using B -band mass dependent PL relations. We will adopt the pulsation modes derived from the theoretical relations for consistency. The mean pulsation masses for $Z=0.001$ are: $\langle M_{FO} \rangle = 1.05 M_{\odot}$ ($\sigma=0.01$), $\langle M_{SO} \rangle = 1.17 M_{\odot}$ ($\sigma=0.02$). For $Z=0.0001$, they are: $\langle M_{FO} \rangle = 0.91 M_{\odot}$ ($\sigma=0.01$), $\langle M_{SO} \rangle = 1.01 M_{\odot}$ ($\sigma=0.01$). These predicted

Table 8. Parameters of the SX Phe stars in Sculptor dSph.

CEMV+2016 name	Original name	Alternative name	RA (J2000)	DEC (J2000)	Period (current)	$\langle B \rangle$	$\langle V \rangle$	$\langle I \rangle$	A_B	A_V	A_I	Q1	Q2
scl-CEMV053	—	—	00 58 52.18	-33 50 13.4	0.08027222	21.638	21.307	20.870	0.414	0.266	0.128	2	0
scl-CEMV138	—	—	00 59 27.90	-33 49 35.4	0.06268482	22.433	22.206	21.683	0.683	0.535	1.098	2	0
scl-CEMV186	—	—	00 59 38.98	-33 50 14.0	0.04709882	22.291	22.134	21.874	0.318	0.279	0.213	2	0
scl-CEMV224	—	—	00 59 47.17	-33 38 16.3	0.07575704	22.138	21.932	21.425	0.437	0.318	0.493	2	0
scl-CEMV227	—	—	00 59 49.29	-33 46 16.6	0.08574464	21.632	21.378	21.096	0.703	0.475	0.386	2	0
scl-CEMV231	—	—	00 59 51.03	-33 41 05.4	0.10634337	21.967	21.624	21.208	0.511	0.511	0.286	2	0
scl-CEMV270	—	—	00 59 56.29	-33 42 00.3	0.05859806	22.491	22.221	21.825	0.450	0.404	0.318	2	0
scl-CEMV285	—	—	00 59 58.67	-33 42 19.8	0.07370760	22.425	22.181	21.775	0.842	0.647	0.503	2	0
scl-CEMV286	—	—	00 59 58.62	-33 50 09.7	0.05043523	22.689	22.516	22.257	0.273	0.320	0.126	2	0
scl-CEMV317	—	—	01 00 03.08	-33 44 46.9	0.06004051	22.515	22.307	22.004	0.845	0.775	0.400	2	0
scl-CEMV325	—	—	01 00 04.57	-33 52 15.4	0.05413676	22.363	22.126	21.793	0.209	0.234	0.174	2	0
scl-CEMV334	—	—	01 00 05.75	-33 43 33.8	0.05398612	22.539	22.248	21.897	0.304	0.253	0.090	2	0
scl-CEMV347	—	—	01 00 07.56	-33 39 51.0	0.05561832	22.726	22.381	22.159	0.631	0.582	0.482	2	0
scl-CEMV364	—	—	01 00 11.00	-33 40 51.2	0.04454330	22.723	22.514	22.181	0.525	0.446	0.226	2	0
scl-CEMV366	—	—	01 00 11.57	-33 41 27.5	0.05656062	22.534	22.184	21.773	0.082	0.326	0.449	2	0
scl-CEMV383	—	—	01 00 15.43	-33 44 05.1	0.09018717	21.689	21.414	21.048	0.350	0.342	0.211	2	0
scl-CEMV394	—	—	01 00 18.03	-33 47 48.5	0.08420236	22.168	21.926	21.596	0.724	0.515	0.398	2	0
scl-CEMV410	—	—	01 00 20.06	-33 46 50.6	0.06548483	21.989	21.796	21.459	0.578	0.473	0.250	2	0
scl-CEMV437	—	—	01 00 28.18	-33 50 11.3	0.06370454	22.434	22.260	21.845	0.592	0.386	0.618	2	0
scl-CEMV500	—	—	01 00 40.84	-33 51 15.3	0.06184286	22.551	22.329	22.051	0.768	0.728	0.399	2	0
scl-CEMV538	—	—	01 00 55.95	-33 31 40.1	0.05790988	22.464	22.173	21.783	0.285	0.236	0.075	2	0
scl-CEMV540	—	—	01 00 56.73	-33 40 14.0	0.06031101	22.659	22.341	22.028	0.303	0.289	0.207	2	0
scl-CEMV541	—	—	01 00 56.60	-33 43 29.8	0.06464694	22.424	22.242	21.854	0.507	0.369	0.439	2	0

See the caption of Table 4 for a description of the Q1 and Q2 parameters.

masses are in good agreement with the evolutionary stellar models (BaSTI, Pietrinferni et al. 2004) as shown in Figure 11. Incidentally, we note that the age of a single star of such a mass is about 4 Gyr. Interestingly, in the star-formation history of *fast* galaxies it is common to detect a peak of star formation at this age, which is interpreted as the contribution of the BSS (Monelli et al. 2010b,a, 2016).

7 OTHER VARIABLE STARS

7.1 Peculiar HB variable stars

We have identified three peculiar variable stars, with periods and LCs similar to those of RRL, but located quite above the HB. They are ~ 0.3 mag brighter than the brightest RRL stars of the *full* sample, but ~ 0.6 mag fainter than the faintest ACs. The properties of these stars, which we could not classify convincingly – see below – are summarized in Table 9, while their LCs are presented in Fig. 12.

From an inspection of the CMD these stars are unlikely to be ACs, which are typically more than 1 mag brighter than the HB in the *V* band. Their location suggests they are either RRL affected by blending or stars evolving off from the blue part of the HB, i.e., stars on the verge to become BL Herculis (BL Her) variables. The first hypothesis is not convincing since these objects are located far from the galaxy centre (see Fig. 2). Furthermore their amplitudes (see Table 9) and their amplitude ratios ($A_B/A_V \sim 1.34$ and $A_V/A_I \sim 1.57$) are similar to that expected for normal RRL stars (Di Criscienzo et al. 2011) thus not supporting a possible blend effect. The second hypothesis is also unlikely, since BL Her typically have periods >1 day (e.g., Wallerstein 2002; Soszyński et al. 2010; Marconi et al. 2011; Soszyński et al. 2015), while these have periods < 0.8 day. Besides, according to the current evolutionary scenario the time spent within the Instability Strip by a star with such a luminosity after the central Helium burning is very short ($<< 10$ Myr; e.g., Pietrinferni et al. 2004), which means that

only in systems with a prominent extreme BHB can we expect to observe BL Her stars (e.g. Maas et al. 2007).

We therefore cannot classify these variables convincingly, but note that similar peculiar objects have been detected in other galaxies (e.g., Carina: Dall’Ora et al. 2003; Coppola et al. 2013, Cetus and Tucana: Bernard et al. 2009).

7.2 Eclipsing binaries

Five eclipsing binaries have been detected. The LCs for five of them are shown in Fig. 13, and the properties are summarized in Table 10. It is worth noting that, for scl-CEMV398, despite the fact that its LC is very similar to one RRc, we classified this star as eclipsing binary based on both the flattening of the brighter part of its LC and on the period ($P=0.474$ d, unusually long for a RRc-type star). Note also the classification provided by Clementini et al. (2005), who classified it as “suspected binary system”.

7.3 Field variable stars

We have identified three variable stars compatible with being foreground field stars. Their LCs are shown in Fig. 14, and the properties are summarized in Table 11. Two are compatible with being field δ Scuti stars.

7.4 Likely candidates

A sizeable sample of 37 LPV and 23 probable variable stars has been detected in Sculptor. For the case of the LPV stars, due to their long periods, a large number of phase points together with an appropriately long temporal coverage are needed to define the shape of their LCs. Despite our large data set, we have not been able to characterize the properties of these stars. We consider a star to be a candidate LPV when we obtain concordant magnitude measurements within individual nights and individual observing runs, but average

Table 9. Parameters of the three *peculiar* variable stars in Sculptor dSph.

CEMV+2016 name	Original name	Alternative name	RA (J2000)	DEC (J2000)	Period (current)	$\langle B \rangle$	$\langle V \rangle$	$\langle I \rangle$	A_B	A_V	A_I	Q1	Q2
scl-CEMV029	—	—	00 58 31.92	-33 58 19.6	0.665435	19.949	19.663	19.135	1.433	1.114	0.648	0	1
scl-CEMV048	V372	—	00 58 50.94	-33 49 31.6	0.4317936	19.885	19.699	19.269	1.021	0.724	0.493	2	0
scl-CEMV482	V152	—	01 00 36.18	-33 45 40.7	0.7305012	20.068	19.716	19.185	1.245	0.931	0.615	0	1

See the caption of Table 4 for a description of the Q1 and Q2 parameters.

Table 10. Parameters of the eclipsing binary stars in Sculptor dSph.

CEMV+2016 name	Original name	Alternative name	RA (J2000)	DEC (J2000)	Period (current)	$\langle B \rangle$	$\langle V \rangle$	$\langle I \rangle$	A_B	A_V	A_I	Q1	Q2
scl-CEMV041	V247	—	00 58 47.11	-33 50 45.2	0.883193:	21.383	20.688	20.051	0.332	0.315	0.600	1	0
scl-CEMV398	K3710	—	01 00 18.65	-33 45 35.1	0.4738299	20.190	19.896	19.418	0.500	0.398	0.263	0	1
scl-CEMV532	V410	—	01 00 51.82	-33 47 55.4	0.960817:	21.266	20.901	20.236	0.414	0.526	0.645	1	0
scl-CEMV582	V315	—	01 01 18.33	-33 43 42.8	0.4363745:	20.214	19.978	19.518	0.504	0.335	0.063	1	0
scl-CEMV584	—	—	01 01 19.77	-33 36 21.0	0.547969:	20.728	20.539	19.633	0.383	0.294	0.974	1	0

See the caption of Table 4 for a description of the Q1 and Q2 parameters.

Table 11. Parameters of the field variable stars found in Sculptor dSph.

CEMV+2016 name	Original name	Alternative name	RA (J2000)	DEC (J2000)	Period (current)	$\langle B \rangle$	$\langle V \rangle$	$\langle I \rangle$	A_B	A_V	A_I	Q1	Q2
scl-CEMV556	—	—	01 01 05.12	-33 46 00.9	0.2784994	19.905	19.488	18.866	0.129	0.108	0.031	4	0
scl-CEMV561	—	—	01 01 06.68	-33 54 46.9	0.06166818	18.408	18.150	17.723	0.234	0.197	0.092	4	0
scl-CEMV600	—	—	01 01 31.04	-33 25 12.4	0.04672141	19.151	18.963	18.651	0.409	0.316	0.188	3	0

See the caption of Table 4 for a description of the Q1 and Q2 parameters.

results from observing runs separated by many months or many years are highly discrepant.

For the case of the probable variables, the insufficient data and the inability to achieve a good light curve makes the classification and the period determination of such stars difficult to do. Based on these facts, we named them “likely candidates”. Table 12 shows the list of these stars. We note that: *i*) 31 out of 37 LPV stars are located near the tip of the RGB; and *ii*) out of the 23 probable variable stars, 4 could be possibly eclipsing binaries, and 2 could be RRc stars.

7.5 Non-variable stars

The comparison with previous work on variable stars in Sculptor discloses that we do not detect any trace of variability in a number of sources previously catalogued as variable, mostly from the van Agt (1978) paper, and a few from the Kaluzny et al. (1995). The list is presented in Table 13.

8 DISCUSSION: THE FAST EARLY CHEMICAL EVOLUTION OF SCULPTOR AND TUCANA

In this work, we presented the most complete and updated catalogue of variable stars in the Sculptor dSph. This is so far one of the largest RRL star samples in external galaxies of similar morphological type. As demonstrated in Paper I, the combination of a large sample together with high quality and multi-band photometry, allowed us to set tight constraints on the metallicity distribution of the old stellar component, and revealed the presence of a significant metallicity spread within the RRL star population ($t > 10$ Gyr). This implies that Sculptor underwent substantial chemical enrichment fast enough to be imprinted in the population we observe today as RRL stars. This manifests itself through a large luminosity spread of the RRL stars (~ 0.35 mag) that

is inconsistent with the evolution of a monometallic population (Paper I). Moreover, we showed that, when splitting the sample of RRL stars according to their luminosity relative to the mean $\langle V \rangle$ mag, the brighter and the fainter subsamples follow different spatial distributions, the latter being more centrally concentrated than the former. If we interpret the bright and faint components in terms of metallicity, the latter is consistent with being more metal-rich. This result is consistent with the spectroscopic results of Tolstoy et al. (2004). This implies that, in agreement with what is generally found in dwarf galaxies, the youngest and chemically more evolved population is located in the innermost regions, surrounded by a more uniform older and more metal-poor one, suggesting a metallicity gradient. In the present work (see § 4.2) we showed that the Bailey diagram is quite complex, with stars populating the region around and intermediate to the typical Oo-I and Oo-II loci. Interestingly, we found that the bright, metal-poor, more extended population preferentially follows the location of the Oo-II (typically more metal-poor) GCs, while the faint, more metal-rich, more centrally concentrated RRL stars have a distribution closer to that of Oo-I clusters.

A surprisingly similar empirical result was found in the Tucana dSph. Bernard et al. (2008) disclosed that the pulsational properties of the RRL stars in this galaxy trace a spatial gradient in the metallicity of its individual stars, which therefore must have appeared very early on in the history of this galaxy. As in Sculptor, fainter RRLs are more centrally concentrated than the brighter RRLs. This was the first time that a spatial variation of pulsational properties was observed in a dwarf galaxy, thanks to the large spatial coverage and number of variables discovered. Fig. 15 compares the Bailey diagram and the period distribution of the RRL stars populations in Sculptor and Tucana. The distribution of the RRab-type shows the same general characteristics, with a large period dispersion at fixed amplitude. This is reflected in the normalized histogram in the lower panel,

Table 12. Parameters of the candidates variable stars with problems of classification in Sculptor dSph.

CEMV+2016 name	Original name	Alternative name	RA (J2000)	DEC (J2000)	Note
scl-CEMV003	V579	—	00 56 29.94	-33 56 03.9	probable variable
scl-CEMV004	V503	—	00 56 32.41	-33 54 52.4	probable variable
scl-CEMV007	V443	—	00 56 57.55	-33 59 20.1	probable variable
scl-CEMV009	—	—	00 57 14.08	-33 48 19.6	probable variable; probable RRc but unable to determine period
scl-CEMV011	V374	—	00 57 37.90	-33 58 57.0	probable variable
scl-CEMV013	—	—	00 57 47.20	-33 31 36.7	probable variable
scl-CEMV017	V546	—	00 57 59.79	-33 55 58.1	probable variable
scl-CEMV023	V581	—	00 58 15.63	-33 47 57.4	probable variable; possible eclipsing binary
scl-CEMV075	—	—	00 59 04.80	-33 38 44.2	LPV
scl-CEMV082	—	—	00 59 08.58	-33 41 52.7	LPV
scl-CEMV101	—	—	00 59 15.76	-33 42 48.6	LPV
scl-CEMV105	—	—	00 59 16.92	-33 40 10.6	LPV
scl-CEMV117	V356	—	00 59 20.53	-33 14 44.2	probable variable
scl-CEMV121	—	—	00 59 23.33	-33 23 48.3	probable variable; possible eclipsing binary
scl-CEMV136	—	—	00 59 27.67	-33 40 35.6	LPV
scl-CEMV140	—	—	00 59 28.28	-33 42 07.4	LPV
scl-CEMV159	—	—	00 59 33.95	-33 38 37.3	LPV
scl-CEMV164	K274	—	00 59 35.36	-33 44 09.4	LPV
scl-CEMV168	—	—	00 59 36.13	-33 44 33.4	LPV
scl-CEMV181	V115	K737	00 59 37.98	-33 42 54.1	probable variable
scl-CEMV194	V204	—	00 59 41.48	-33 51 36.8	probable variable; multimode?
scl-CEMV196	V539	—	00 59 42.42	-33 46 57.9	probable variable; possible eclipsing binary, but unable to determine period
scl-CEMV203	—	—	00 59 43.15	-33 56 46.7	LPV
scl-CEMV221	K687	—	00 59 46.40	-33 41 23.4	LPV
scl-CEMV228	—	—	00 59 49.18	-33 58 25.2	LPV
scl-CEMV241	—	—	00 59 52.27	-33 44 54.7	LPV
scl-CEMV244	—	—	00 59 53.00	-33 39 19.0	LPV
scl-CEMV254	V97	—	00 59 54.63	-33 43 42.6	LPV
scl-CEMV289	V544	—	00 59 58.92	-33 28 35.0	LPV
scl-CEMV296	—	—	01 00 00.06	-33 38 34.3	LPV
scl-CEMV303	V551	—	01 00 01.13	-33 59 21.3	probable variable
scl-CEMV343	V80	—	01 00 06.15	-33 50 36.5	LPV
scl-CEMV346	—	—	01 00 07.56	-33 37 03.8	LPV
scl-CEMV368	—	—	01 00 12.12	-33 37 25.9	LPV
scl-CEMV372	K4780	—	01 00 13.97	-33 37 32.9	probable variable; possible detached eclipsing binary
scl-CEMV395	—	—	01 00 18.19	-33 31 40.4	LPV
scl-CEMV412	—	—	01 00 20.72	-33 45 18.0	LPV
scl-CEMV450	—	—	01 00 30.74	-33 37 30.5	LPV
scl-CEMV460	—	—	01 00 32.35	-33 31 57.8	LPV
scl-CEMV462	V575	—	01 00 32.83	-33 38 32.4	probable variable, period near 1d
scl-CEMV469	—	—	01 00 34.03	-33 39 04.6	LPV
scl-CEMV503	—	—	01 00 41.77	-33 51 40.8	possible variable, but unable to determine period; possibly near 1d
scl-CEMV504	—	—	01 00 42.55	-33 35 47.4	LPV
scl-CEMV530	—	—	01 00 50.86	-33 45 05.3	LPV
scl-CEMV534	—	—	01 00 52.13	-33 41 27.1	probable variable
scl-CEMV550	—	—	01 01 02.87	-33 38 52.2	LPV
scl-CEMV566	—	—	01 01 08.54	-33 45 34.9	LPV
scl-CEMV573	—	—	01 01 14.54	-33 30 09.2	LPV
scl-CEMV578	—	—	01 01 17.33	-33 37 05.1	LPV
scl-CEMV586	—	—	01 01 20.82	-33 53 04.7	LPV
scl-CEMV591	—	—	01 01 24.58	-33 38 34.5	LPV
scl-CEMV595	—	—	01 01 26.93	-33 41 44.7	probable variable; probable RRc but unable to determine period
scl-CEMV607	—	—	01 01 39.09	-33 56 38.5	LPV
scl-CEMV608	—	—	01 01 39.58	-33 45 04.3	LPV
scl-CEMV613	—	—	01 01 49.41	-33 54 10.2	LPV
scl-CEMV615	V480	—	01 01 54.54	-34 05 21.7	probable variable
scl-CEMV628	V530	—	01 02 44.13	-33 25 54.4	probable variable
scl-CEMV629	V577	—	01 02 45.21	-33 46 36.4	probable variable
scl-CEMV631	—	—	01 02 52.67	-33 37 26.9	probable variable
scl-CEMV633	V587	—	01 03 43.20	-34 23 34.3	probable variable

which clearly shows that the period coverage is essentially the same.

Indeed, the old population of the two systems presents striking similarities, which are unique among the low-mass galaxies of the LG. No other dSph investigated so far shows such clear evidence of chemical evolution imprinted in their population of RRL stars. This may suggest that the early conditions of the two galaxies, and in particular the mass and star formation histories may have been similar, in order to explain that both systems were able to retain enough nucleosynthesis products to provide early enrichment as observed today. Nonetheless, Sculptor and Tucana also exhibit important differences.

At present, Tucana is a very isolated dSph at the edge of the Local Group (~ 870 kpc from the MW versus ~ 84 kpc for Sculptor). Given its current location in the Local Group and its relatively high recession velocity, Tucana seems to have been an isolated Local Group galaxy during the majority of its lifetime, except perhaps for a close encounter with the MW or M31 at early epochs (Fraternali et al. 2009). On the contrary, with an apogalactic distance of 122 kpc and orbital period of 2.2 Gyr (Piatek et al. 2006), Sculptor spent most of its existence within the halo of the MW. Under these conditions, theoretical investigations indicate that tidal stripping, stirring, and ram-pressure stripping (Blitz & Robishaw 2000;

Table 13. Parameters of non-variable stars in Sculptor dSph.

Original name	Alternative name	RA (J2000)	DEC (J2000)	Note
V573	—	00 56 38.63	-33 25 23.7	not variable?
V397	—	00 57 24.12	-33 38 02.5	not variable?
V580	—	00 57 33.20	-33 52 00.2	not variable?
V596	—	00 57 49.52	-33 32 23.3	not variable?
V559	—	00 58 12.31	-33 37 50.4	not variable?
V547	—	00 58 36.48	-34 02 11.9	not variable?
V252	—	00 58 45.65	-33 32 12.8	not variable
V251	—	00 59 00.13	-33 38 50.9	not variable
V311	—	00 59 21.44	-33 48 48.6	not variable?
V332	—	00 59 32.85	-33 57 44.4	not variable
V554	—	00 59 35.22	-33 29 04.3	not variable?
K403	—	00 59 36.61	-33 46 05.7	not variable
V416	—	00 59 44.35	-33 55 19.3	not variable?
V200	—	00 59 47.20	-33 33 37.0	not variable?
V382	—	00 59 57.66	-33 46 56.5	not variable?
V370	—	01 00 06.99	-33 52 25.7	not variable?
V173	—	01 00 17.17	-33 56 06.4	not variable
V60	—	01 00 21.78	-33 39 07.7	no bright star here; estimated position is 11.4 arcseconds from K4313
V245	—	01 00 24.43	-33 25 09.7	not variable
V558	—	01 00 24.75	-33 51 06.6	not variable?
V557	—	01 00 26.14	-33 41 07.3	not variable?
V54	—	01 00 28.99	-33 51 52.5	not variable
K5081	—	01 00 30.78	-33 46 27.1	not variable?
V45	—	01 00 39.78	-33 52 21.9	not variable
V532	—	01 00 43.79	-33 29 08.1	not variable?
V424	—	01 00 47.84	-33 58 54.2	not variable?
V340	—	01 01 21.98	-33 42 22.6	not variable?
V571	—	01 02 36.69	-33 30 07.1	not variable?
V307	—	01 03 23.63	-33 44 16.8	not variable?

Mayer et al. 2006), as well as the local UV radiation from the primary galaxy (Mayer et al. 2007) all act to remove dark matter and/or baryons from the dwarf, implying that satellite galaxies such as Scl may have been up to ten times more massive in the past (Kravtsov et al. 2004). However, Sculptor is considerably more massive than Tucana at the present time ($M_V = -11.1$ versus -9.6 for Tucana). If Sculptor had been ten times as massive as we observe it today, the mass-metallicity relation would suggest a larger increase in metallicity at early times. However, this is in contrast with the lack of HASP RRL stars, which are solid tracers of an old stellar population more metal-rich than $[\text{Fe}/\text{H}] \gtrsim -1.5$. Moreover, Coleman et al. (2005) demonstrated that beyond the tidal radius (from both photometric and spectroscopic data) there is no evidence of extra-tidal structure, suggesting the absence of strong tidal interaction. This argues against substantial mass loss along Sculptor’s history and may suggest that, possibly, Sculptor has quietly and passively evolved during its revolutions around the Milky Way. The similarity of the stellar populations of Sculptor and Tucana, including at early times, provides support to the scenario about the origin of the dwarf galaxy types introduced by Gallart et al. (2015), in which dwarf galaxy types may be imprinted by the early conditions of formation rather than only being the result of a recent or secular morphological transformation driven by environmental effects. In this particular case, both Sculptor and Tucana may have formed in the relatively high density environment close to the centre of what would become the Local Group, and this would be instrumental in becoming *fast* galaxies, i.e., galaxies whose star formation history is dominated by an early and short star formation event, with little star formation afterwards. The subsequent sustained interaction of Sculptor with the Milky Way would have had a minor effect in its star formation history and mass characteristics, and thus Sculptor and Tucana remain

galaxies with similar mass and star formation history today despite the substantially different secular evolution.

9 SUMMARY AND CONCLUSIONS

We have presented the largest catalogue (so far) of variable stars in the Sculptor dSph galaxy. This work is based on the homogeneous photometric analysis of 4,404 images in the *B*, *V*, and *I* bands collected over 24 years in 21 different observing runs and using 6 different telescopes and 7 different instruments, employing the same methodologies as the “Homogeneous Photometry” series. The main results of this work are:

- Basic properties (period, amplitude, mean magnitude, position) have been made available for all the stars, together with the light curves and the finding charts (see Appendix A).
- In total, we have discovered 147 variable stars in the calibrated portion of the Sculptor dSph, among which 81 are RRLs, 23 SX Phe, one *peculiar*, one eclipsing binary and 38 “likely candidates” (31 of them are probable LPV stars, one is a possible eclipsing binary, two are probable RRc and four more are possible variables of uncertain type).
- Out of the 634 detected variables in the current work, 334 (301 RRLs) have their periods identified for the first time, and 354 (320 RRLs) have their pulsation parameters also given for the first time.
- We have detected 536 RR Lyrae variable stars. Out of these, 289 are RRab type stars, 197 are RRc, and 50 stars are suspected RRd double-mode pulsators. We have discussed the distribution of stars in the Bailey diagram, showing that the metallicity spread among RRL stars discussed in Paper I reflects not only in the luminosity spread

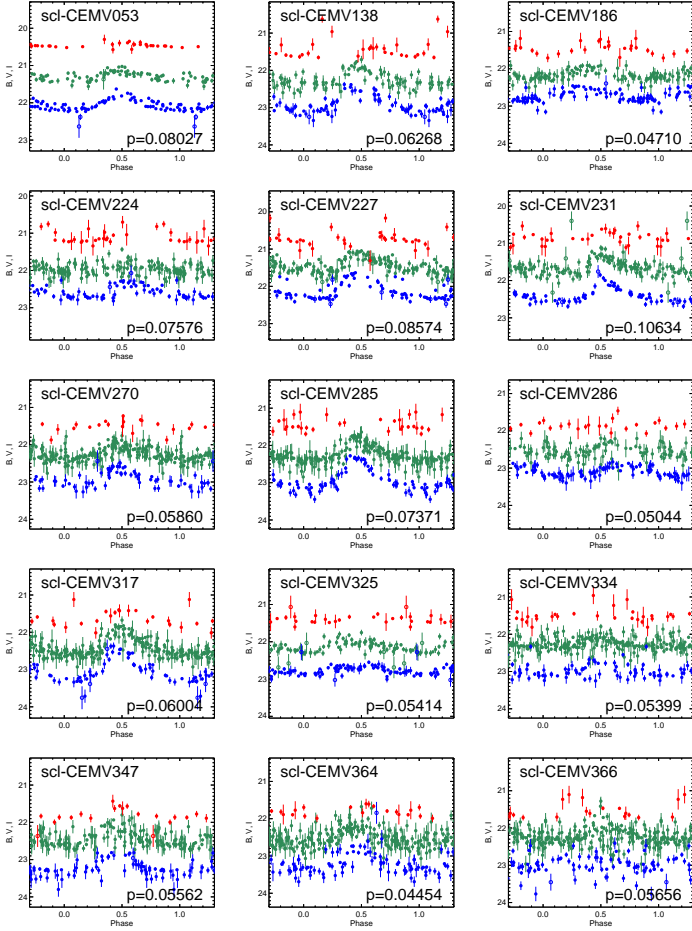


Figure 9. Sample of light curves of the SX Phe stars in the B (blue), V (green) and I (red) bands, phased with the period in days given in the lower right-hand corner of each panel. The name of the variable is given in the left-hand corner of each panel. Open symbols show the bad data points, i.e., with discrepancies larger than 3σ above the standard error of a given star; these were not used in the calculation of the period and mean magnitudes. For clarity, the B and I light curves have been shifted by 0.4 mag down- and upward, respectively. Beige backgrounds mark those SX Phe stars classified as within the *clean* sample. All light curves are available as Supporting Information with the online version of the paper.

of the HB, but also in the broad period distribution that covers both Oo-I and Oo-II loci as well as the intermediate regions and in the amplitude range for a given period;

- We have confirmed the existence of four ACs over the surveyed area. We have derived the pulsation mode and the mass of each of them, which is close to $1.5 M_{\odot}$ for all.

- We have discussed 23 newly discovered SX Phe stars. Using theoretical models developed by (Fiorentino et al. 2015b), and the distance derived from RRLs in Paper I, we classified them as 16(17) FO, 6(5) SO, assuming a mean metallicity of $Z=0.001$ ($Z=0.0001$). On the other hand, the empirical relations by McNamara (2011) instead suggest that 15(13) are F and 5(5) are FO. The discrepancy come

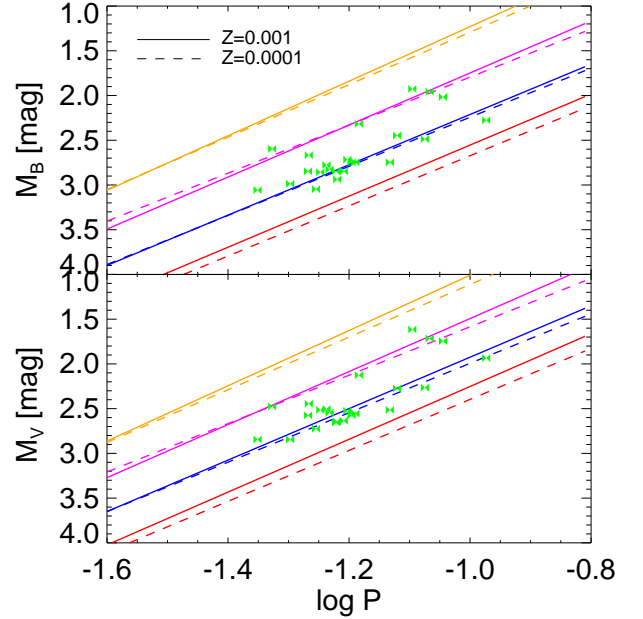


Figure 10. Absolute M_B (top) and M_V (bottom) period-luminosity diagrams with theoretical PL relation of SX Phe stars for $Z=0.001$ (solid lines) and $Z=0.0001$ (dashed lines). The colours red, blue, magenta and orange indicate the F, FO, SO, TO pulsation modes, respectively, of the previous relations. Green bow-tie symbols shows the 23 SX Phe found in Sculptor dSph in this work. They were plotted assuming a true distance modulus of 19.62 mag (Paper I) and a reddening of 0.018 mag (Pietrzynski et al. 2008) plus the reddening law from Cardelli et al. (1989).

from the zero-point offset (~ 0.3 mag) between both relations. The mean mass derived for them is of about $1 M_{\odot}$. If we assume that the entire sample of SX Phe comes from single star evolution, they might indicate a residual star formation $\simeq 4$ Gyr ago, or coalescence of very low mass stars.

- We also discuss the existence of three *peculiar* variable stars, located in the region of the CMD between the RRL star and the ACs, which have pulsation properties inconsistent with other classes of variable brighter than the HB, such as the BL Her stars. Their nature remains unclear.

- Five eclipsing binaries and 37 probable long period variables, and a few (3) field variable stars were also presented.

We have discussed the striking similarities between the properties of the old population in the Sculptor and Tucana dSph galaxies, which are imprinted in the complex populations of their RRL stars. Despite the large spatial coverage of the present work ($\sim 2.5 \text{ deg}^2$), a complete investigation of stellar variability over the full tidal radius of Sculptor is still lacking. Moreover, a direct confirmation of the metallicity spread among the RRL population through spectroscopic follow-up could provide further insight into the early chemical evolution of this galaxy. The future development of this project does require new precise and radial velocity

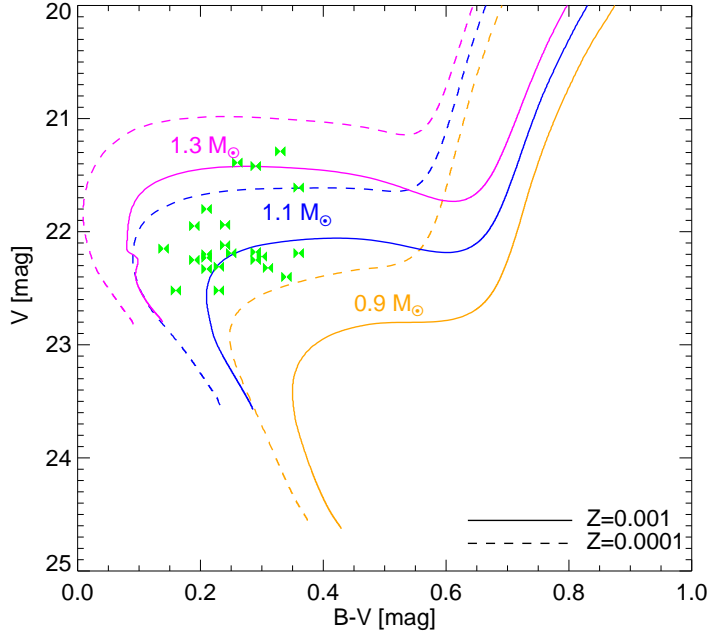


Figure 11. Distribution of the 23 SX Phe stars in Sculptor dSph in the optical ($B-V$, V) CMD (with the same colour code as in Fig. 1). We have represented the standard scaled-solar evolutionary tracks from the BaSTI library (Pietrinferni et al. 2004) for different metallicities $Z=0.001$ (solid lines) and $Z=0.0001$ (dashed lines), and for the masses $0.9 M_{\odot}$ (orange lines), $1.1 M_{\odot}$ (blue lines) and $1.3 M_{\odot}$ (magenta lines).

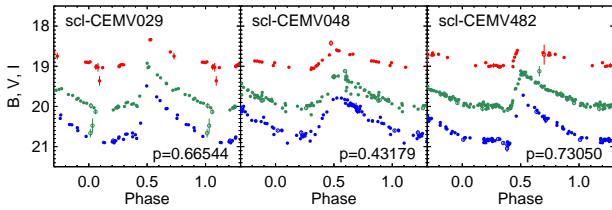


Figure 12. Sample of light curves of the peculiar variable stars in the B (blue), V (green) and I (red) bands, phased with the period in days given in the lower right-hand corner of each panel. The name of the variable is given in the left-hand corner of each panel. Open symbols show the bad data points, i.e., with errors larger than 3σ above the mean error of a given star; these were not used in the calculation of the period and mean magnitudes. For clarity, the B and V light curves have been shifted by 0.4 mag down- and upward, respectively.

measurements of both RG and HB stars to assess whether the two different populations show different kinematics and different chemical enrichment histories as recently suggested by (Fabrizio et al. 2015, 2016 AJ accepted) for Carina dSph. Note that the quoted approach took advantage of the c_{UBI} index to separate stellar populations along the RGB. This means that deep and accurate U-band photometry is also urgently required.

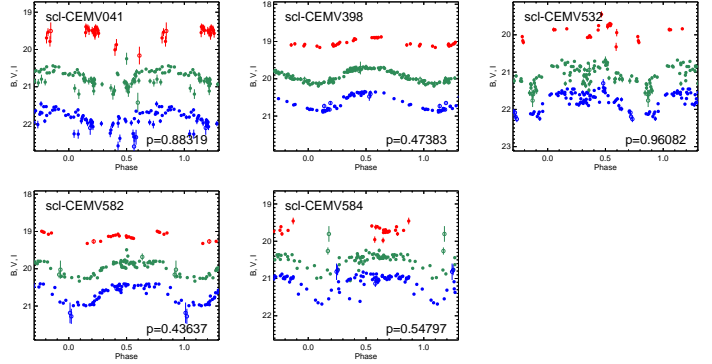


Figure 13. Sample of light curves of the eclipsing binary stars in the B (blue), V (green) and I (red) bands, phased with the period in days given in the lower right-hand corner of each panel. The name of the variable is given in the left-hand corner of each panel. Open symbols show the bad data points, i.e., with errors larger than 3σ above the mean error of a given star; these were not used in the calculation of the period and mean magnitudes. For clarity, the B and I light curves have been shifted by 0.4 mag down- and upward, respectively.

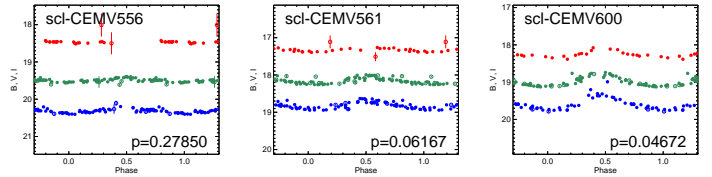


Figure 14. Sample of light curves of the field variable stars in the B (blue), V (green) and I (red) bands, phased with the period in days given in the lower right-hand corner of each panel. The name of the variable is given in the left-hand corner of each panel. Open symbols show the bad data points, i.e., with errors larger than 3σ above the mean error of a given star; these were not used in the calculation of the period and mean magnitudes. For clarity, the B and I light curves have been shifted by 0.4 mag down- and upward, respectively.

ACKNOWLEDGMENTS

We thank the referee for his/her comments, careful reading and detailed report. CEM-V is grateful to the Rome Observatory and the Physics Department of the Tor Vergata University where part of this work has been carried out. CEM-V acknowledges the support by the ULL through a grant funded by the Agencia Canaria de Investigación, Innovación y Sociedad de la Información and co-funded by the Fondo Social Europeo (FSE) under the framework of Programa Operativo de Canarias (POC 2007-2013). This research has been supported by the Spanish Ministry of Economy and Competitiveness (MINECO) under the grant (project reference AYA2014-56795-P). EJB acknowledges support from the CNES postdoctoral fellowship program. GF has been supported by the Futuro in Ricerca 2013 (grant RBFR13J716).

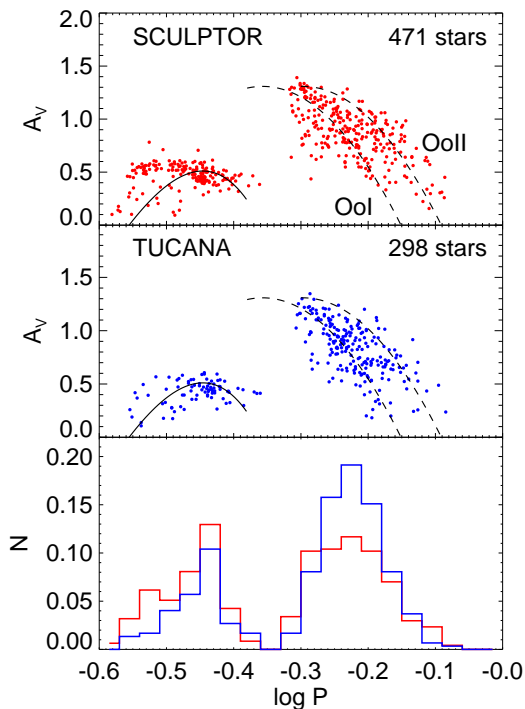


Figure 15. Top. Period- V amplitude diagram for Sculptor (top) and Tucana (middle, Bernard et al. 2009). For clarity, RRd stars do not appear in these diagrams, which only consider stars with well defined pulsational properties. The bottom panel shows the normalized distribution of RRab and RRc stars in both galaxies (red: Sculptor, blue: Tucana).

REFERENCES

- Baade W., Hubble E., 1939, *PASP*, **51**, 40
 Bernard E. J., et al., 2008, *ApJ*, **678**, L21
 Bernard E. J., et al., 2009, *ApJ*, **699**, 1742
 Bernard E. J., et al., 2010, *ApJ*, **712**, 1259
 Bernard E. J., et al., 2013, *MNRAS*, **432**, 3047
 Blazhko S., 1907, *Astronomische Nachrichten*, **175**, 327
 Blitz L., Robishaw T., 2000, *ApJ*, **541**, 675
 Bono G., Caputo F., Santolamazza P., Cassisi S., Piersimoni A., 1997a, *AJ*, **113**, 2209
 Bono G., Caputo F., Cassisi S., Incerpi R., Marconi M., 1997b, *ApJ*, **483**, 811
 Cacciari C., Corwin T. M., Carney B. W., 2005, *AJ*, **129**, 267
 Canterna R., 1976, *AJ*, **81**, 228
 Caputo F., Cassisi S., Castellani M., Marconi G., Santolamazza P., 1999, *AJ*, **117**, 2199
 Cardelli J. A., Clayton G. C., Mathis J. S., 1989, *ApJ*, **345**, 245
 Cassisi S., Salaris M., 2013, Old Stellar Populations: How to Study the Fossil Record of Galaxy Formation
 Castellani V., degl'Innocenti S., 1995, *A&A*, **298**, 827
 Catelan M., 2009, *Ap&SS*, **320**, 261
 Clementini G., Ripepi V., Bragaglia A., Martinez Fiorenzano A. F., Held E. V., Gratton R. G., 2005, *MNRAS*, **363**, 734
 Coleman M. G., Da Costa G. S., Bland-Hawthorn J., 2005, *AJ*, **130**, 1065
 Coppola G., et al., 2013, *ApJ*, **775**, 6
 Coppola G., et al., 2015, *ApJ*, **814**, 71
 Cusano F., et al., 2015, *ApJ*, **806**, 200
 Da Costa G. S., 1984, *ApJ*, **285**, 483
 Dall'Ora M., et al., 2003, *AJ*, **126**, 197
 Demarque P., Hirshfeld A. W., 1975, *ApJ*, **202**, 346
 Di Criscienzo M., et al., 2011, *AJ*, **141**, 81
 Fabrizio M., et al., 2015, *A&A*, **580**, A18
 Ferraro F. R., et al., 2012, *Nature*, **492**, 393
 Fiorentino G., Monelli M., 2012, *A&A*, **540**, A102
 Fiorentino G., Limongi M., Caputo F., Marconi M., 2006, *A&A*, **460**, 155
 Fiorentino G., Lanzoni B., Dalessandro E., Ferraro F. R., Bono G., Marconi M., 2014, *ApJ*, **783**, 34
 Fiorentino G., et al., 2015a, *ApJ*, **798**, L12
 Fiorentino G., Marconi M., Bono G., Dalessandro E., Ferraro F. R., Lanzoni B., Lovisi L., Mucciarelli A., 2015b, *ApJ*, **810**, 15
 Fraternali F., Tolstoy E., Irwin M. J., Cole A. A., 2009, *A&A*, **499**, 121
 Gallart C., Aparicio A., Freedman W. L., Madore B. F., Martínez-Delgado D., Stetson P. B., 2004, *AJ*, **127**, 1486
 Gallart C., et al., 2015, *ApJ*, **811**, L18
 Garofalo A., et al., 2013, *ApJ*, **767**, 62
 Harbeck D., et al., 2001, *AJ*, **122**, 3092
 Hirshfeld A. W., 1980, *ApJ*, **241**, 111
 Hurley-Keller D., Mateo M., Grebel E. K., 1999, *ApJ*, **523**, L25
 Irwin M., Hatzidimitriou D., 1995, *MNRAS*, **277**, 1354
 Kaluzny J., Kubiak M., Szymanski M., Udalski A., Krzeminski W., Mateo M., 1995, *A&AS*, **112**, 407
 Kirby E. N., Guhathakurta P., Bolte M., Sneden C., Geha M. C., 2009, *ApJ*, **705**, 328
 Kravtsov A. V., Gnedin O. Y., Klypin A. A., 2004, *ApJ*, **609**, 482
 Kuehn C., et al., 2008, *ApJ*, **674**, L81
 Kunder A., et al., 2013, *AJ*, **146**, 119
 Layden A. C., Ritter L. A., Welch D. L., Webb T. M. A., 1999, *AJ*, **117**, 1313
 Maas T., Giridhar S., Lambert D. L., 2007, *ApJ*, **666**, 378
 Majewski S. R., Siegel M. H., Patterson R. J., Rood R. T., 1999, *ApJ*, **520**, L33
 Mapelli M., Ripamonti E., Battaglia G., Tolstoy E., Irwin M. J., Moore B., Sigurdsson S., 2009, *MNRAS*, **396**, 1771
 Marconi M., Fiorentino G., Caputo F., 2004, *A&A*, **417**, 1101
 Marconi M., Bono G., Caputo F., Piersimoni A. M., Pietrinferni A., Stellingwerf R. F., 2011, *ApJ*, **738**, 111
 Marconi M., et al., 2015, *ApJ*, **808**, 50
 Martínez-Vázquez C. E., et al., 2015, *MNRAS*, **454**, 1509
 Martínez-Vázquez C. E., et al., 2016, *MNRAS*, **461**, L41
 Mateo M. L., 1998, *ARA&A*, **36**, 435
 Mayer L., Mastropietro C., Wadsley J., Stadel J., Moore B., 2006, *MNRAS*, **369**, 1021
 Mayer L., Kazantzidis S., Mastropietro C., Wadsley J., 2007, *Nature*, **445**, 738
 McConnachie A. W., 2012, *AJ*, **144**, 4
 McNamara D. H., 2000, *PASP*, **112**, 1096
 McNamara D. H., 2011, *AJ*, **142**, 110
 Monelli M., et al., 2010a, *ApJ*, **720**, 1225
 Monelli M., et al., 2010b, *ApJ*, **722**, 1864
 Monelli M., et al., 2016, *ApJ*, **819**, 147
 Monkiewicz J., et al., 1999, *PASP*, **111**, 1392
 Norris J., Zinn R., 1975, *ApJ*, **202**, 335
 Oosterhoff P. T., 1939, *The Observatory*, **62**, 104
 Ordoñez A. J., Sarajedini A., 2016, *MNRAS*, **455**, 2163
 Petersen J. O., Christensen-Dalsgaard J., 1999, *A&A*, **352**, 547
 Piatek S., Pryor C., Bristow P., Olszewski E. W., Harris H. C., Mateo M., Minniti D., Tinney C. G., 2006, *AJ*, **131**, 1445
 Pietrinferni A., Cassisi S., Salaris M., Castelli F., 2004, *ApJ*, **612**, 168
 Pietrzynski G., et al., 2008, *AJ*, **135**, 1993
 Poleski R., et al., 2010, *Acta Astron.*, **60**, 1
 Poretti E., et al., 2008, *ApJ*, **685**, 947
 Pych W., Kaluzny J., Krzeminski W., Schwarzenberg-Czerny A., Thompson I. B., 2001, *A&A*, **367**, 148

- Reimers D., 1975, *Memoires of the Societe Royale des Sciences de Liege*, **8**, 369
- Renzini A., Mengel J. G., Sweigart A. V., 1977, *A&A*, **56**, 369
- Rizzi L., 2002, PhD thesis, University of Padova, Italy
- Santolamazza P., Marconi M., Bono G., Caputo F., Cassisi S., Gilliland R. L., 2001, *ApJ*, **554**, 1124
- Shapley H., 1938, *Harvard College Observatory Bulletin*, **908**, 1
- Sills A., Karakas A., Lattanzio J., 2009, *ApJ*, **692**, 1411
- Skúladóttir Á., Tolstoy E., Salvadori S., Hill V., Pettini M., Shetrone M. D., Starkenburg E., 2015, *A&A*, **574**, A129
- Smith H. A., Stryker L. L., 1986, *AJ*, **92**, 328
- Soszyński I., Udalski A., Szymański M. K., Kubiak M., Pietrzyński G., Wyrzykowski L., Ulaczyk K., Poleski R., 2010, *Acta Astron.*, **60**, 91
- Soszyński I., et al., 2015, *Acta Astron.*, **65**, 233
- Starkenburg E., et al., 2013, *A&A*, **549**, A88
- Stetson P. B., 1987, *PASP*, **99**, 191
- Stetson P. B., 1994, *PASP*, **106**, 250
- Stetson P. B., 1996, *PASP*, **108**, 851
- Stetson P. B., 2000, *PASP*, **112**, 925
- Stetson P. B., 2005, *PASP*, **117**, 563
- Stetson P. B., Hesser J. E., Smecker-Hane T. A., 1998a, *PASP*, **110**, 533
- Stetson P. B., et al., 1998b, *ApJ*, **508**, 491
- Stetson P. B., Bruntt H., Grundahl F., 2003, *PASP*, **115**, 413
- Stetson P. B., Catelan M., Smith H. A., 2005, *PASP*, **117**, 1325
- Stetson P. B., Fiorentino G., Bono G., Bernard E. J., Monelli M., Iannicola G., Gallart C., Ferraro I., 2014, *PASP*, **126**, 616
- Swope H. H., 1968, *The Astronomical Journal Supplement*, **73**, 204
- Thackeray A. D., 1950, *The Observatory*, **70**, 144
- Tolstoy E., et al., 2004, *ApJ*, **617**, L119
- Wallerstein G., 2002, *PASP*, **114**, 689
- Wallerstein G., Cox A. N., 1984, *PASP*, **96**, 677
- Welch D. L., Stetson P. B., 1993, *AJ*, **105**, 1813
- de Boer T. J. L., et al., 2011, *A&A*, **528**, A119
- de Boer T. J. L., et al., 2012, *A&A*, **539**, A103
- van Agt S. L. T. J., 1978, *Publications of the David Dunlap Observatory*, **3**, 205

APPENDIX A: FINDING CHART

Fig. A1 displays a mosaic centred on Sculptor dSph, divided in 56 quadrants. In the electronic version we show finding charts for each quadrant in which we found variable stars. In this way, we make available the finding charts for the whole sample of variable stars detected. Fig. A2 shows the finding chart for the 28 quadrant of the mosaic of Sculptor (Fig. A1). The labelled numbers are those belonging to the numerical suffix from our assigned names (scl-CEMV+suffix).

This paper has been typeset from a $\text{\TeX}/\text{\LaTeX}$ file prepared by the author.

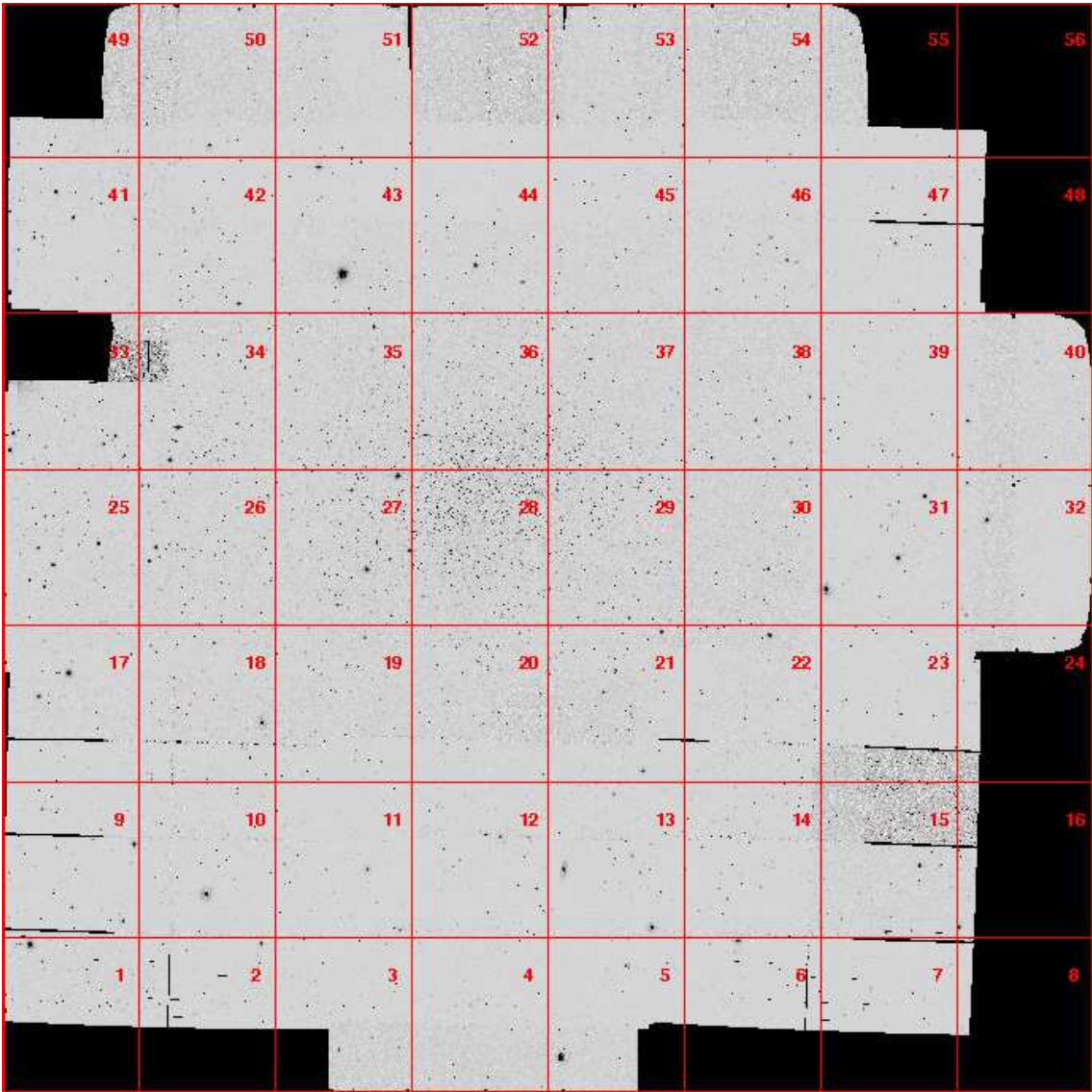


Figure A1. Mosaic of Sculptor.

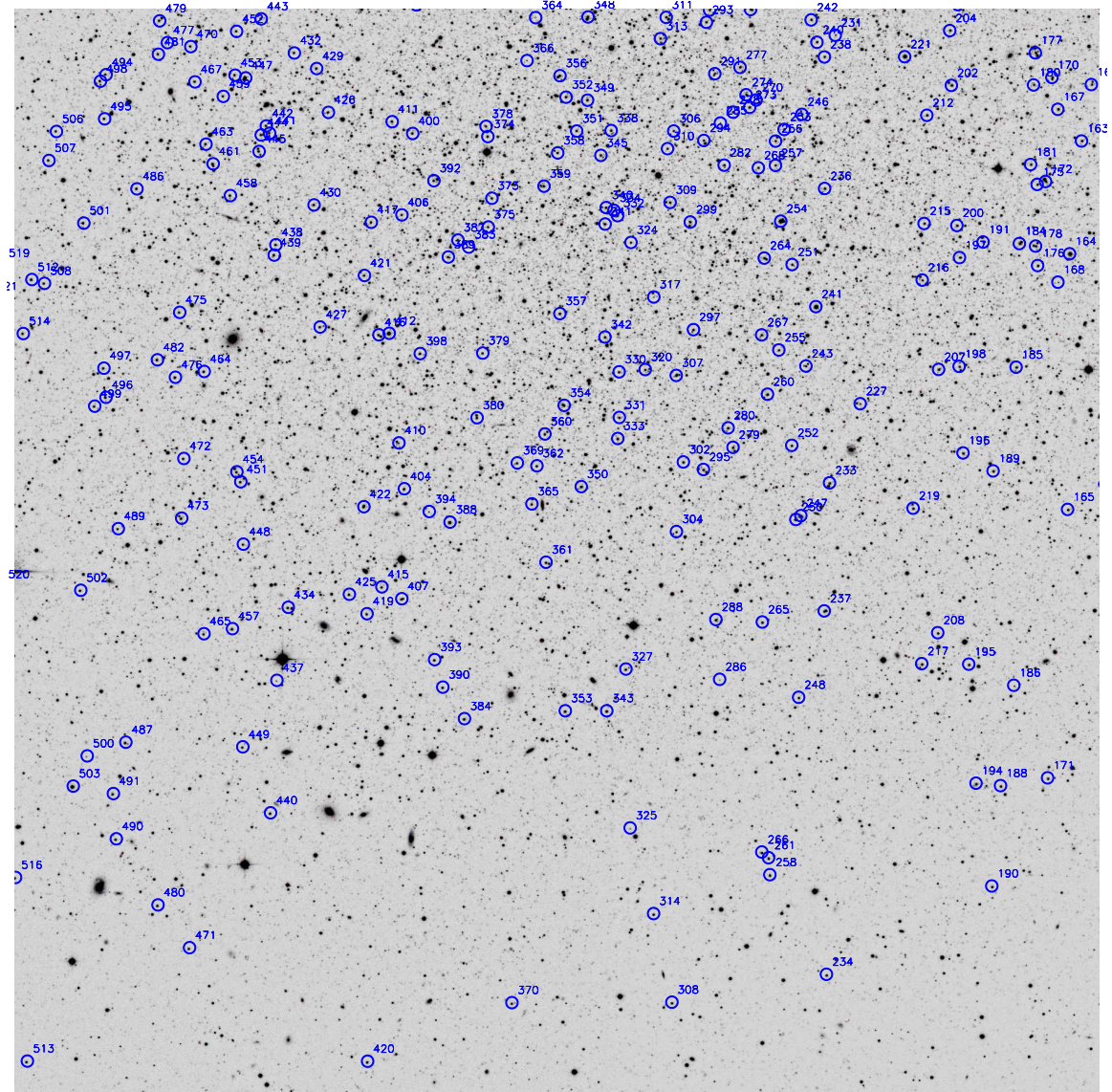


Figure A2. Finding chart for the quadrant 28 of the Mosaic of Sculptor (A1). North is up and east to the left. The labelled numbers correspond to the numerical suffix from our assigned names (scl-CEMV+suffix). The other quadrants are in the electronic edition.